FUNCTIONAL RETINAL GANGLION CELL ACTIVITY FOLLOWING LIGHT-INDUCED RETINAL DAMAGE IN MICE

by

Jezreel Justine Sy

Submitted in partial fulfillment of the requirements
for the degree of Master of Science

at

Dalhousie University
Halifax, Nova Scotia
March 2019

Table of Contents

List of Tables

List of Figures

Abstract

The scotopic threshold response (STR) of the electroretinogram (ERG) is thought to measure inner retinal function, specifically retinal ganglion cells (RGCs). However, the degree to which the STR is masked by the larger amplitudes of outer retinal function is not known. Light-induced retinal damage (LIRD) was used to selectively cause photoreceptor death in pigmented and albino mice to examine whether the effects of phototoxicity extend beyond photoreceptors. In pigmented mice, there was no structural loss measured with optical coherence tomography over a 121-day period, however, there was a decrease in ERG function. In albino mice, we found retinal thickness loss over a 73-day period, which correlated with the much larger decrease in outer retinal function. No RGC loss was observed with either strain. Changes in inner retinal function are much larger in albino compared to pigmented mice despite no structural loss, suggesting that there are other underlying mechanisms affecting the RGC function indirectly via the loss of photoreceptors, and thereby the generation of the STR.

List of Abbreviations Used

cGMP – cyclic guanine monophosphate

dH_20 – distilled water

ELM – external limiting membrane

ERG – electroretinogram

H&E – hematoxylin & eosin

GCL – ganglion cell layer

ILM – inner limiting membrane

INL – inner nuclear layer

IPL – inner plexiform layer

LIRD – light induced retinal damage

min – minute(s)

nSTR – negative scotopic threshold response

OCT – optical coherence tomography

ONL – outer nuclear layer

OPL – outer plexiform layer

PBS – phosphate buffered saline

PCL – photoreceptor cell layer

pSTR – positive scotopic threshold response

RBPMS – RNA binding protein with multiple splicing

RNFL – retinal nerve fiber layer

RGC – retinal ganglion cells

ROI – region of interest

RPE – retinal pigment epithelium

s – second(s)

STR – scotopic threshold response

Acknowledgements

I gratefully acknowledge the many contributions to this project by the members of the Retina Lab. In particular, I would like to thank Michele Hooper, Janette Nason, Corey Smith and Ben Smith for the training and technical assistance in running my experiments. In addition, I thank Spring Farrell for her guidance and suggestions for writing my thesis. A special note of gratitude goes to my supervisor Dr. Balwantray Chauhan, as well as to my committee members Dr. Francois Tremblay and Dr. Jeremy Murphy for providing high quality scientific training, direction and encouragement throughout my graduate training. I also thank my Clinical Vision Science family for their guidance and support. To all of you, I offer my deep appreciation.

1. Chapter 1: Introduction

1.1. The retina

The retina is a thin layer of neural tissue (approximately 200-320μm thick in humans (Kolb, 2007); similarly, approximately 204μm thick in wild-type mice (Ferguson et al., 2013) that is responsible for converting light energy into visual information. It is located between the choroid and the vitreous, and extends from the circular edge of the optic disc to the ora serrata. When light enters the eye, photons travel through the cornea, aqueous, lens, vitreous, and penetrates the entire retina before reaching the photoreceptors. From there, photoreceptors transform light energy into electrical signals, which are then passed on via a series of neural connections to second and third order neurons and relayed via the optic nerve to the brain.

1.1.1. Retinal tissue organization

The retina (Figure 1-1) is a complex structure made up of several specialized cells arranged in a highly organized manner. Histologically, they appear as ten distinct layers (Table 1-1) that include three layers of cell bodies (outer nuclear layer, inner nuclear layer and ganglion cell layer) and two layers of synapses (outer plexiform layer and inner plexiform layer).

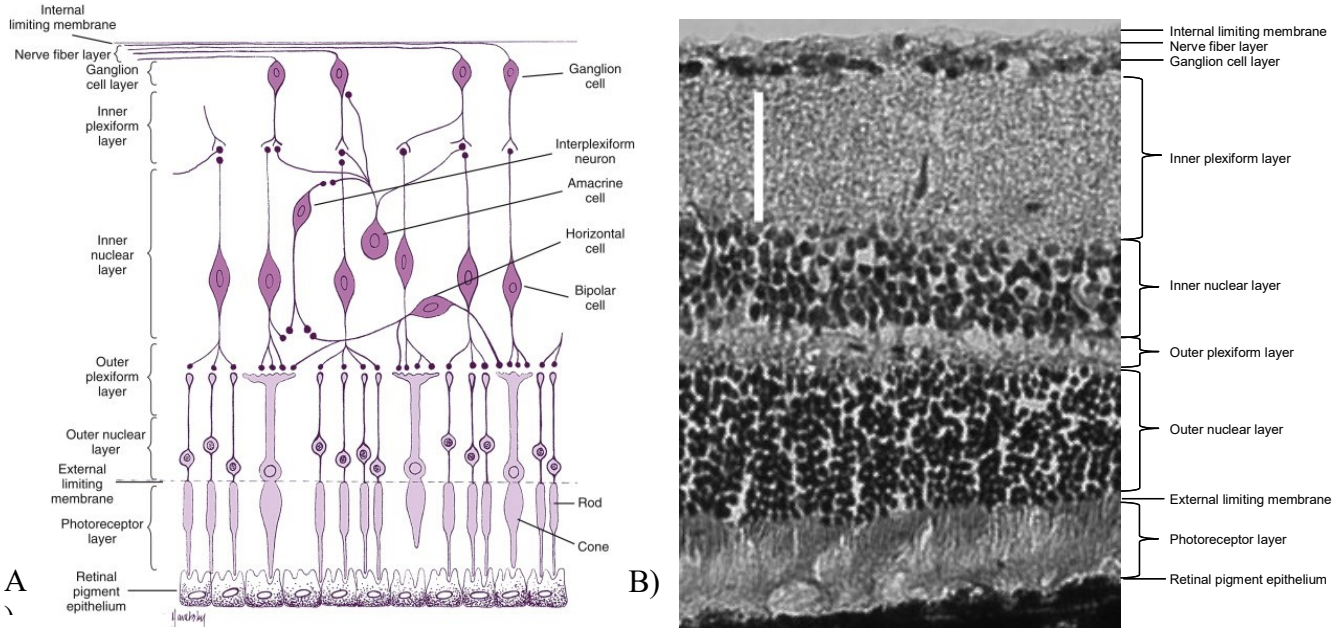

Figure 1-1. The retina contains highly specialized cells intricately arranged in 10 distinct layers. A) Schematic of the retina (Reprinted from Clinical Anatomy and Physiology of the Visual System (p. 71) from by L. A. Remington, 2012, St. Louis: Butterworth-Heinemann. Copyright [2012] by Butterworth-Heinemann. Reprinted with permission.) and B) light micrograph of a C57BL/6 mouse retina (scale bar = 50μm, magnification = 20x).

The retinal pigment epithelium (RPE) consists of a single layer of pigmented cells. While not part of the neural retina, and has several important functions, including retina adhesion, nutrient/waste exchange, light absorption, phagocytosis of rod outer segment discs, immune privilege and protection from oxidative stress (Thumann et al., 2013). The RPE also plays a role in the visual cycle (discussed in Section 1.1.2) by storing vitamin A and recycling all-*trans* retinol to 11-*cis*-retinal through a transporter system (Thumann et al., 2013).

When light strikes the eye, specialized neurons, called photoreceptors (rods and cones), absorb photons of light and convert them to electrical potentials in a

process called phototransduction. Most mammals have retinas where rods predominate. There are approximately 115 million rods and 6.5 million cones in the human retina, with the rod and cone densities varying in different regions of the retina. The periphery is rod-dominated (30,000 rods/mm^2), while cone density increases towards the macula. The specialized region for critical vision called the fovea and is dominated by cones (150,000 cones/mm^2) (Forrester et al., 2016). Rodents such as mice and rats do not have an area for centralized vision called the fovea, although they similarly have a central retina with a higher concentration of photoreceptors compared to the periphery. Compared to the human retina, the mouse retina has a larger number of photoreceptors per area (Volland et al., 2015). Being nocturnal animals, mice and rats have retinas that are overwhelmingly dominated by rods. Their cones are small in size and only make up 3-5% of the total number of photoreceptors (Kolb, 2003). At the lowest levels of light (scotopic conditions), only the rods are activated. These cells are responsible for detecting contrast, motion and brightness, however they have poor resolution and spatial discrimination (Purves & Williams, 2004). Cone photoreceptors operate in the ranges of mid to bright light intensities and are responsible for the perception of fine detail, spatial resolution and colour vision (Forrester et al., 2016). Mesopic vision occurs at levels of light where both rods and cones are activated, such as during twilight. Cone photoreceptors start contributing to visual perception at the level of starlight, and become more dominant as the level of illumination is increased (Purves & Williams, 2004). In bright light (photopic conditions), the

contribution of rods to visual perception is reduced almost entirely because their response to light saturates and vision is mediated by the cone photoreceptors.

The electrical potentials generated by photoreceptors travel along a vertical pathway to bipolar cells, whose main function is to transmit the visual signal from the photoreceptors to the retinal ganglion cells (RGC). The ratio of cones : bipolar cells : RGCs can be 1 : 1 : 1 in the central retina in humans; whereas in the peripheral retina, bipolar cells can receive stimuli from as many as 50-100 rods (Forrester et al., 2016). This summation of stimuli accounts for the high sensitivity of rods in responding to dim illumination. There are two types of bipolar cells: ON-type and OFF-type. ON-type bipolar cells are stimulated by the photoreceptor response to increased illumination, and play a role in detecting light images against a dark background. In contrast, OFF-type bipolar cells are stimulated by the photoreceptor response to a decrease in illumination, and play a role in detecting dark images against a light background (Kolb, 2003). RGCs are the output neurons of the retina, and mainly function in integrating inputs received from bipolar and amacrine cells to form highly pre-processed information to be sent to higher visual centers in the brain. RGCs have receptive fields arranged in concentric circles that are either ON-center or OFF-center. In ON-center RGCs, stimulating the center of the receptive field produces an agonistic response while stimulating the periphery of the receptive field produces an antagonistic response. Conversely in OFF-center RGCs, stimulating the center of the receptive field produces an antagonistic response while stimulating the periphery of the receptive field produces an agonistic response (Purves & Williams, 2004). Axons from the RGCs make up the retinal nerve fiber

layer (RNFL) and exit the eye in bundles, forming the optic nerve. Amacrine cells, horizontal cells and interplexiform neurons modulate and integrate the visual signal before it is transmitted to the brain. Neuroglial cells (which include Müller cells, microglial cells and astrocytes) do not actively participate in the transmission of the visual signal but play a role in the structure, support and immune function of the retina (Remington, 2012).

Table 1-1. Layers of the retina, arranged from outermost to innermost

Layer	Description
Retinal pigment epithelium (RPE)	Outermost boundary of the retina composed of a single layer of RPE cells (Remington, 2012).
Photoreceptor cell layer (PCL)	Outer and inner segments of rod and cone photoreceptors (Remington, 2012).
External limiting membrane (ELM)	Zonula adherens junctions between photoreceptor cells, as well as the zonula adherens junctions between the photoreceptor cells and Müller cells (Remington, 2012).
Outer nuclear layer (ONL)	Cell bodies of the rod and cone photoreceptors that are arranged in several rows (8-10 cells thick in humans, Sharma & Ehinger, 2003; 11.5 ± 1.3 cells thick in mice, Wang et al., 2014).
Outer plexiform layer (OPL)	Synaptic processes between the ONL and the INL. This is where rods and cones interact with bipolar cell dendrites and horizontal cell processes (Remington, 2012).
Inner nuclear layer (INL)	Cell bodies of horizontal cells, bipolar cells, amacrine cells, interplexiform neurons, Müller cells and displaced RGCs (Remington, 2012).
Inner plexiform layer (IPL)	Synaptic processes between the INL and GCL. This is where bipolar cells interact with amacrine cells and RGCs (Gregg, McCall, & Massey, 2013).
Ganglion cell layer (GCL)	Cell bodies of RGCs and displaced amacrine cells (Gregg et al., 2013).
Retinal nerve fiber layer (RNFL)	RGC axons (Remington, 2012).
Inner limiting membrane (ILM)	Innermost boundary of the retina composed of Müller cell footplates covered by a basement membrane (Remington, 2012).

1.1.2. The role of rhodopsin in the visual cycle

The visual process begins when visual pigment molecules found in photoreceptor cells detect a light signal. In rods, the photopigment rhodopsin makes up more than 90% of the protein mass found in the disc membranes of outer segments (Molday, 1998; Palczewski, 2014) and is responsible for initiating scotopic vision (Park, 2014). Rhodopsin is made up of the protein opsin covalently attached to 11-*cis*-retinal, a light sensitive chromophore derived from vitamin A. When photoactivated, 11-*cis*-retinal is released and transformed to all-*trans*-retinal, changing the configuration of the rhodopsin molecule. This initiates the phototransduction cascade whereby light is converted to an electrical signal. The changed configuration then limits the degree to which rods are stimulated and decreases their sensitivity to bright light. This renders the rods inactive until rhodopsin regeneration can take place. The activated rhodopsin is then broken down and all-trans-retinal is transported from the outer segment to the RPE, where enzymes convert it back to 11-*cis*-retinal. It is then transported back to the outer segment discs where it recombines with opsin, thus completing the rhodopsin cycle (Purves & Williams, 2004). In the dark, rhodopsin levels gradually increase until sensitivity to light is regained.

1.1.3. Signal propagation

The series of biochemical alterations in the rhodopsin molecule that occurs upon light absorption activates the intracellular messenger transducin, which in turn activates a phosphodiesterase that hydrolyzes nucleotide cyclic guanosine

monophosphate (cGMP). cGMP regulates the number of ion channels in the outer segment membrane that open or close, allowing Na^+ and Ca^{2+} ions to flow into the cell. In the dark, high levels of cGMP levels keep the voltage-gated Ca^{2+} channels open, allowing more neurotransmitter release from the synaptic terminals of the photoreceptor. The photoreceptors remain in a relatively depolarized state, where the membrane potential is approximately -40mV. Introducing the photoreceptor to progressively increasing illumination causes the cGMP levels drop and the ion channels to close. The membrane potential becomes more negative and induces a graded hyperpolarization of the photoreceptor, ultimately leading to the reduction of glutamate release at the photoreceptor synapse (Purves & Williams, 2004) and the visual signal is then relayed to the bipolar cells. OFF-type bipolar cells contain ionotropic glutamate receptors that respond to glutamate binding by opening voltage-dependent Na^+, K^+ and Ca^{2+} ion channels, leading to graded depolarization of the cell. ON-type bipolar cells contain metabotropic glutamate receptors (mGluR6), which indirectly close voltage-dependent ion channels via a biochemical cascade (Westheimer, 2007). The release of glutamate from bipolar cells to the RGCs triggers the opening of voltage-dependent Na^+ channels and results in depolarization of the RGC dendrites, which then triggers an action potential to the brain via the optic nerve. The changes in membrane potential involved in the relay of the visual signal are accompanied by electrical currents that flow in the extracellular space, giving rise to voltages that can be recorded.

1.2. Electroretinogram

The electroretinogram (ERG) is a non-invasive diagnostic test that measures the mass electrical activity of the retina in response to light stimulation by using electrodes to record the corneal potential. Clinically, the ERG is used to provide an objective assessment of total retinal function, and is used to confirm the diagnosis of retinal degenerations, toxic retinopathy, metallosis, or generalized retinal dysfunction (Jiménez-Sierra, Ogden, & Van Boemel, 1989). In general, when retinal function deteriorates, the electrical activity following light stimulation is reduced, thus resulting in a smaller ERG and indicating retinal pathology (Perlman, 2018). This makes it a useful method in monitoring disease progression and in evaluating the effectiveness of therapeutic interventions. Experimentally, the ERG changes in a characteristic way in response to increased retinal illumination, and is therefore a useful method for studying retinal function in the laboratory and clinic.

1.2.1. Components of the dark-adapted full-field (Ganzfeld) ERG

A full-field ERG uses a diffuse flash to uniformly illuminate the whole visual field. The resulting ERG waveform is a composite signal consisting of several component "waves" that can be traced to specific cells or cell types in the retina that originate from different stages of retinal processing (Frishman, 2013; Pinto et al., 2007). The scotopic ERG is primarily dominated by the rod pathway. There are multiple factors that influence the magnitude of contribution of different retinal cell types to the ERG. Retinal neurons that are radially oriented to the cornea (i.e. photoreceptors, bipolar cells) make larger contributions to the ERG wave than laterally oriented

neurons (i.e. horizontal and amacrine cells) (Frishman & Wang, 2011). Other factors such as stimulus strength and wavelength, level of background illumination, duration and spatial extent of the stimulus, and the location of the stimulus within the visual field all additionally influence contribution to the ERG (Frishman, 2013).

For the purposes of this thesis, only the a-wave, b-wave and scotopic threshold response (STR) components of the scotopic ERG are discussed. The typical ERG response consists of an initial negative a-wave followed by a positive b-wave (Figure 1-2 A). The a-wave corresponds to photoreceptor function. Early experiments with intraretinal ERG recordings from cats and rats have demonstrated that the a-wave originates from the outer segments of photoreceptors (Brown & Wiesel, 1961; Penn & Hagins, 1969). Inducing photoreceptor death, such as in models of light induced retinal damage (LIRD), results in a reduction of the a-wave (Grimm & Remé, 2013; Reuter & Hobbelen, 1977). A reduced a-wave is also found in mice with abnormal outer segments (Rhodopsin knockout mice) (Toda et al., 1999). The b-wave primarily reflects activity of the bipolar cells. Pharmacologically blocking the synaptic transmission between photoreceptors and bipolar cells causes a reduction in the b-wave (Pepperberg et al., 1978). Clinically, it has been found that mutations that cause a defect in the synaptic transmission between photoreceptors and bipolar cells, such as in human congenital stationary night blindness, result in a lack of b-wave while retaining a normal or near-normal a-wave (Baker & Kerov, 2013; Kolb, 2003). With very weak flashes, the a- and b-waves of the fully dark-adapted retina disappear, and the STR dominates the ERG.

The STR (Figure 1-2 B) corresponds to the functional activity of the inner retina, with particular contributions from RGCs. Intraretinal recordings in the cat demonstrate that the STR originates in the proximal retina (Sieving, Frishman, & Steinberg, 1986). In mice, the STR contains a slow negative potential, the negative STR (nSTR), that is preceded by a positive potential, the positive STR (pSTR) (Saszik et al., 2002). Pharmacological suppression of the inner retinal cells in mice suppresses both the pSTR and nSTR (Saszik et al., 2002). Studies of optic nerve crush and transection in mice and rats show that the pSTR component is more severely affected by the RGC loss than the nSTR component (Alarcon-Martinez et al., 2009; Smith et al., 2014). In mice, cats and humans, the nSTR is not completely eliminated by RGC loss (Sieving, 1991; Smith et al., 2014), and could be mediated more by amacrine cells (Frishman, 2013).

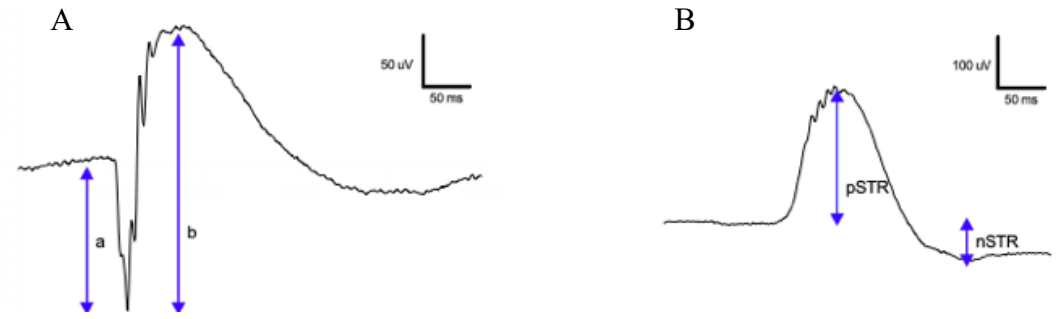

Figure 1-2. A) The ERG response of a dark-adapted C57BL/6 mouse following a bright flash (1.0 log cd s m^{-2}). The first negative potential is the a-wave (a), followed by the positive potential b-wave (b). B) The STR is elicited with a weak flash (-3.2 log cd s m^{-2}) and shows the positive component pSTR followed by the negative component nSTR.

1.3. Optical coherence tomography (OCT)

The OCT is a non-invasive imaging technique that uses low-coherence interferometry to produce a two-dimensional image of optical scattering from internal tissue microstructures (Huang et al., 1991). In the eye, the OCT is often used to obtain high-resolution cross-sectional images of the retina (Figure 1-3). Recent advances in OCT technology allow real-time eye tracking to avoid motion artifact and can even register the location so that subsequent scans can be obtained in the identical location and compared to the initial scan.

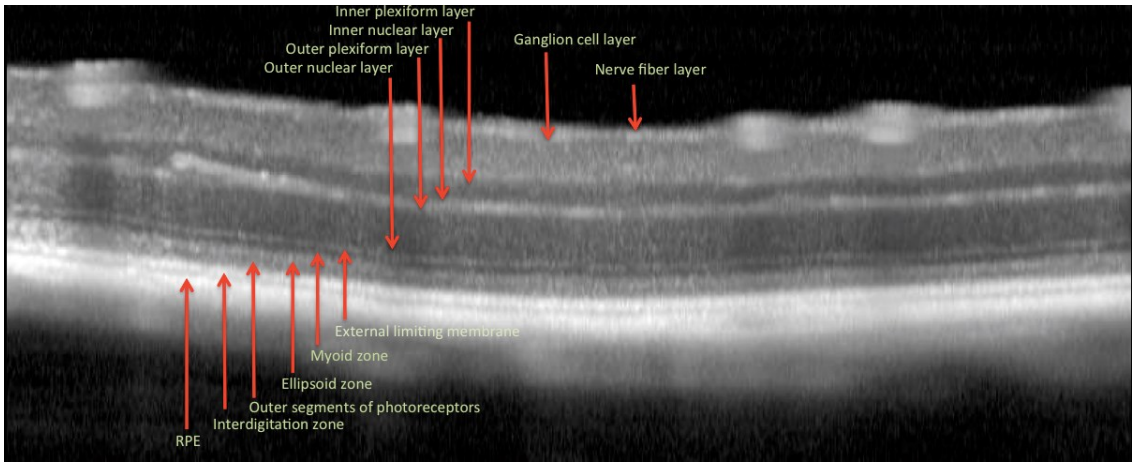

Figure 1-3. OCT scan of a C57BL/6 mouse 12 degrees from the optic nerve head. Each tissue layer exhibits different degrees of reflectance, allowing visualization of the different retinal layers.

1.4. Light-induced retinal damage (LIRD)

LIRD is a well-documented method used to selectively cause photoreceptor loss through light exposure (Grimm & Remé, 2013). In a landmark study by Noell et al. (1966), it was discovered that continuous exposure of albino rats to ambient light caused irreversible damage to the retina. LIRD has been found to cause functional and structural changes in the retina. Histological studies confirm a loss in the

thickness of the outer nuclear layer (Wasowicz et al., 2002) that is even evident with *in vivo* imaging of the retinal layers with OCT (Bhavna et al., 2017). Unsurprisingly, photoreceptor cell loss corresponded to a decrease in the a-wave ERG (Sugawara, Sieving, & Bush, 2000). The severity of damage caused by LIRD is dependent on a variety of factors, including the intensity and duration of light exposure (Organisciak & Vaughan, 2010), wavelength of light (Vicente-Tejedor et al., 2018; Putting et al., 1994), age of animal (Polosa, Bessaklia, & Lachapelle, 2017), presence of ocular pigmentation (Wasowicz et al., 2002), circadian rhythms, and rearing light environments (Organisciak & Vaughan, 2010).

1.4.1. Mechanisms of damage

Long-term exposure to lower wavelengths of light results in the generation of free radicals, leading to photochemical damage (Youssef, Sheibani, & Albert, 2010). During LIRD, bleaching of rhodopsin leads to shedding of the outer segment discs and shortening of the outer segments. Normally rhodopsin is regenerated via the rhodopsin cycle and new discs eventually replace the shed discs. In models of LIRD however, the rapid rate of rhodopsin bleaching and regeneration is thought to play a role in the pathological signalling for apoptosis in the outer retina (Organisciak & Vaughan, 2010) due to phagocytosis of massively shed outer segment disks and oxidative stress to the RPE (Remé et al., 1998; Saenz-de-Viteri et al., 2014; Miceli et al., 1994). Indeed, mutated mice with decreased capacity for rhodopsin regeneration show an increased resistance to light damage (Wenzel et al., 2001). Morphological signs of apoptosis, such as condensation of nuclear chromatin and

rod inner segments can be observed as early as 20 minutes after LIRD in albino BALB/c mice (Wenzel et al., 2001). This is followed by a gradual loss of photoreceptor cells, invasion of macrophages and a final scar formation (Remé et al., 1998). Most of the damage is limited to ONL, leaving an intact inner retina (Remé et al., 1998).

Under white light, the primary chromophore affected by light damage is rhodopsin (Grimm et al., 2001; Grimm et al., 2000). Absorption of radiation energy by chromophores in the retina and RPE causes the generation free radicals, which occurs in one of two ways. In the first one, light absorption causes the excitation of electrons from a ground state to an excitation state. This raises the level of energy at the level of the atom and leads to a state of instability. In order to return to the more stable ground state, some atoms simply release the energy they have absorbed. However in some instances, the higher energy level of the excited state is used to split molecular bonds by electron or hydrogen exchange, leading to the formation of free radicals. In the second way, light absorption causes a direct transfer of energy from the excited chromophore to oxygen. These free radicals cause tissue damage by breaking down molecules via protein and lipid oxidation. Retinal photoreceptors in particular contain a large concentration of membranous structures, making them susceptible to damage by free radicals (Youssef et al., 2010).

1.4.2. Murine models of LIRD

Nocturnal rodents such as mice and rats have widely been used in studies of retinal phototoxicity. In these animals LIRD is largely confined to the rod

photoreceptors, and the subsequent retinal cell loss is restricted to the outer nuclear layer (Organisciak & Vaughan, 2010). Topographical preferential ONL loss due to LIRD has been found in the superior and temporal retina by some groups (Tanito et al., 2008; Marco-Gomariz et al., 2006; Montalbán-Soler et al., 2012; García-Ayuso et al., 2011). Exposure to light intensities only 2-3 times above normal (1,200-2,500 lux) room lighting is sufficient to cause retinal damage (Noell et al., 1966), making them convenient to use in studies of LIRD.

1.5. Presentation of the problem and purpose of the study

RGCs are central nervous system neurons that transmit visual information from the retina into the brain, and injury to these cells can result in vision loss (Levin & Gordon, 2002). Currently, there are very few methods that can be used to specifically quantify RGC function. In human optic nerve disease such as glaucoma, the STR has not been found to be a reliable measure of RGC function (Korth et al., 1994), and other measures such as the photopic negative response of the full-field ERG (Gotoh et al., 2004) and the pattern ERG (Ganekal et al., 2013) are more useful in detecting RGC dysfunction in humans. The STR however has been successfully used in rodent experimental models of glaucoma to monitor changes in RGC function following optic nerve injury (Alarcón-Martínez et al., 2009; Alarcón-Martínez et al., 2010; Smith et al., 2014). It is important however to analyze separately the contributions from all retinal cells and circuits that combine to form the composite ERG waveform. Contributions from other cells, particularly the photoreceptors, can alter the downstream STR response and lead to an

overestimation of RGC contribution to the overall ERG waveform (Saszik et al., 2002; Smith et al., 2014). By eliminating photoreceptor contribution, we can determine how this impacts RGC function and the overall retinal function.

The present study examines how structural changes in LIRD correlates with functional changes in the retina. Based on how the visual signal is relayed, we can surmise that complete elimination of the photoreceptor contribution will result in a flat STR because none of the signals originating from the photoreceptors will reach the RGCs. However if only a partial loss of photoreceptors is induced, we can determine whether the loss of photoreceptor function is proportional to the loss of inner retinal function.

Previous research in mice and rats employing LIRD showed that in addition to the expected reduction of the a-wave amplitude caused by the loss of photoreceptors, there was also a reduction in the STR (García-Ayuso et al., 2011; Montalbán-Soler et al., 2012; Sugawara et al., 2000). García-Ayuso et al. showed that LIRD causes RGC loss (proposed to be due to axonal compression caused by changes in retinal vasculature after LIRD) and a permanent loss of the STR in albino rats (García-Ayuso et al., 2011). Other studies involving albino rats and mice however showed no loss of RGCs despite a reduced STR (Montalbán-Soler et al., 2012; Sugawara et al., 2000). Furthermore, some recovery of the a-wave and the STR was found post-LIRD in albino mice (Montalbán-Soler et al., 2012). Thus, it remains unclear whether the STR reduction after LIRD is due to a loss of RGCs or if there are other underlying mechanisms that are responsible.

Previous studies (García-Ayuso et al., 2011; Montalbán-Soler et al., 2012; Sugawara et al., 2000) that examined how the STR changes after LIRD relied on histology in order to determine structural loss. One limitation of using histology is that individual animals cannot be followed longitudinally. As well, poorly processed specimens can be prone to artefacts such as shrinkage, tears and excessive separation of layers, leading to inaccurate representations of tissue morphology as they exist *in vivo* (Rastogi et.al., 2013). Recent advances in OCT technology have allowed us to visualize the retinal layers *in vivo* and in great detail to provide a way to reliably measure changes in retinal thickness in the same individuals over time.

The present study aims to determine how LIRD affects RGC function by characterizing the STR response based on the amount of photoreceptor loss in a mouse model. We hypothesize that the functional loss of photoreceptor activity due to LIRD has a corresponding proportional functional loss of inner retinal activity. We utilize ERG and OCT to longitudinally assess retinal function and structure respectively, and retinas are then harvested for immunohistochemical analysis. These analyses will correlate a-wave and STR reductions with retinal thickness loss and determine whether functional deficits in the ERG reflect cell loss.

2. Chapter 2: Methods

2.1. Overview of protocol

The effect of phototoxicity on the mouse retina structure and function was examined. ERGs and OCTs were obtained at baseline, prior to LIRD treatment. After LIRD, follow-up ERGs and OCTs were obtained in regular intervals up to Day 121. OCTs were captured in a subset of mice at early time points (Day 1, 3 and 7) to assess structural loss shortly after LIRD. At the end of the experiment, the mice were sacrificed and the eyes were harvested. Photoreceptors and RGCs were quantified using immunohistochemical methods. A subset of mice was sacrificed at Day 7 for a histologic examination of the retina at an intermediate timepoint.

2.2. Light induced retinal damage treatment

A description of the lightbox apparatus used for the LIRD treatment is as follows: 14 white fluorescent bulbs (Sylvania Fluorescent T8 32W Daylight Bulb) provided 22,000 lux of light exposure, as measured with a luxmeter, from overhead and from the sides. A mirror was placed beneath the cages for maximum light exposure from below. A fan was used to provide ventilation and to prevent mice from becoming overheated.

Prior to LIRD treatment, mice were dark-adapted overnight (≥12 hours). Both eyes were dilated with 1 drop 1% atropine sulphate (Bausch & Lomb, Laval, QC, Canada) and 1% cyclopentolate hydrochloride (Bausch & Lomb). After ensuring mydriasis, the mice were individually placed in clear acrylic cages with a metal grill

top with food and water. They were then placed in the lightbox apparatus for duration of 12 hours. Throughout the light exposure duration, pupils were regularly checked to ensure mydriasis was maintained and additional dilating drops were reapplied when necessary. New stimuli (such as food, toys, or exposure to scents from other mice) were introduced every two hours in an effort to keep the mice engaged and to prevent them from falling asleep. The light intensity was checked during regular intervals to ensure that the same intensity was maintained throughout the duration of light exposure.

2.3. Animals

The protocols were approved by the Dalhousie University Committee on Laboratory Animals, and all procedures were performed in accordance with regulations established by the Canadian Council on Animal Care. A total of 18 C57BL/6 mice and 13 BALB/c mice were used in this study.

Pigmented C57BL/6 (Strain code 027) and albino BALB/c (Strain code 028) mice between 8 and 16 weeks of age were purchased from Charles River Laboratories (Saint-Constant, QC, Canada), and housed at the Carleton Animal Care Facility at Dalhousie University. Mice were kept in standard cages with unlimited access to food and water in a 12-hour light/dark cycle environment.

2.4. Electroretinogram

2.4.1. Animal preparation

Mice were dark adapted overnight (≥12 hours) for scotopic ERG acquisition and subsequently handled under dim red light. Mice were anesthetized with a mixture of ketamine (100mg/kg body weight, Vetoquinol, Georges Lavaltrie, QC, Canada) and xylazine (10 mg/kg body weight, Bayer Inc., Misssisauga, ON, Canada) in saline solution that was injected intraperitoneally. Both eyes were dilated topically with 1 drop tropicamide (Bausch & Lomb) and 1 drop 1% cyclopentolate hydrochloride (Bausch & Lomb). The reference and ground electrodes (Grass Instruments, Quincy, MA, USA) were placed subdermally in the forehead and hind leg, respectively. The measuring electrodes (DTL Plus Electrode, Diagnosys, Littleton, MA, USA) were positioned on the cornea after a drop of Tear-Gel (Novartis Pharmaceuticals, Mississauga, ON, Canada) was added, and a contact lens was placed over it (See Figure 2-1). The body temperature was maintained at 37°C by a heating pad and monitored through rectal temperature feedback. Following setup, mice were allowed to stabilize for an additional 10 minutes before acquisition of the recordings.

A 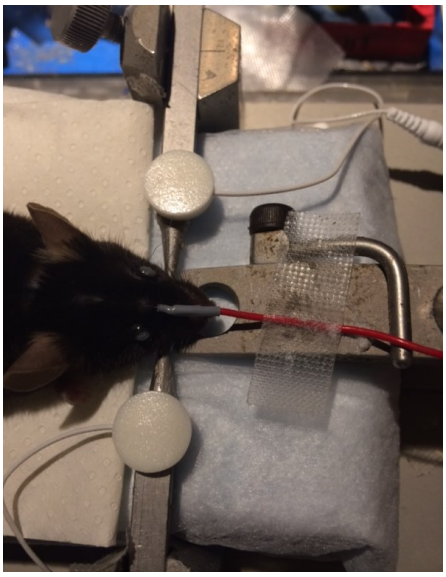 B 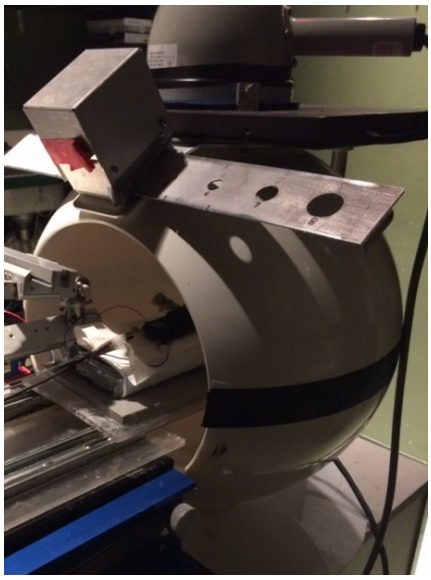

Figure 2-1. Mouse ERG setup. (A) The ERG signal is recorded from corneal electrodes. Subdermal reference and ground electrodes were placed on the forehead and hind leg, respectively. (B) The mouse was positioned inside a Ganzfeld bowl for the duration of the recording. ERG recordings were performed in complete darkness.

2.4.2. Recordings

Flashes were delivered through a Ganzfeld stimulator (LKC Technologies, Gaithersburg, MD, USA) with a maximum illumination of 1.0 log cd s/m^2. Stimulus strengths were attenuated by up to 6.2 log units by manual interposition of neutral density filters (Kodak Wratten, Rochester, NY, USA). The interval time between flash stimuli varied from 4.5 s at the dimmest illumination to 20 s at the brightest illumination. 2-40 responses were averaged depending on the stimuli strength. Both photopic and scotopic responses were amplified 10,000-fold, filtered (1–300 Hz bandwidth, P511 AC Amplifier, Grass Instruments), and digitized using LabVIEW 9.0 dedicated software (National Instruments, Austin, TX, USA).

2.4.3. Data analysis

Analysis of ERG waveforms was completed using a custom ERG analysis toolbox written for Matlab (Mathworks, Natick, MA, USA). Waveforms were filtered with a low pass Butterworth filter at 50 Hz to remove high frequency oscillatory potentials. Baseline was set for 100 ms, which corresponded to the onset of the flash stimulus. For ERG responses acquired from dim flash stimuli (-3.2 to -5.2 log cd s/m^2), the pSTR amplitude was measured from baseline to the maximum positive peak and the nSTR was measured from baseline to the maximum negative trough. For ERG responses acquired from bright flash stimuli (1.0 to -2.4 log cd s/m^2), the a-wave amplitude was measured from the baseline to the maximum negative trough and the b-wave was measured from the a-wave trough to the maximum positive peak.

2.5. Optical Coherence Tomography

In vivo imaging was performed with spectral domain optical coherence tomography (OCT) device (Spectralis Multiline, Heidelberg Engineering GmbH, Heidelberg, Germany) modified for use in mice (Chauhan et al., 2012). Due to the configuration of the OCT device, scans were only taken from the left eye.

2.5.1. Animal preparation

For each mouse, the left eye was dilated topically with 1 drop tropicamide and 1 drop 1% cyclopentolate hydrochloride. Mice were anesthetized with inhalant 1.5-2% volume isoflurane (Baxter Corporation, Mississauga, ON, Canada) with 1.5 L/min oxygen flow delivered through a nose cone attached to a portable

inhalation system (See Figure 2-2). The body temperature was maintained at 37°C by a heating pad. Tear-Gel (Novartis Pharmaceuticals) and a custom-made polymethyl methacrylate plano contact lens (Cantor and Nissel Limited, Brackley, UK) were used to maintain corneal hydration and improve image quality.

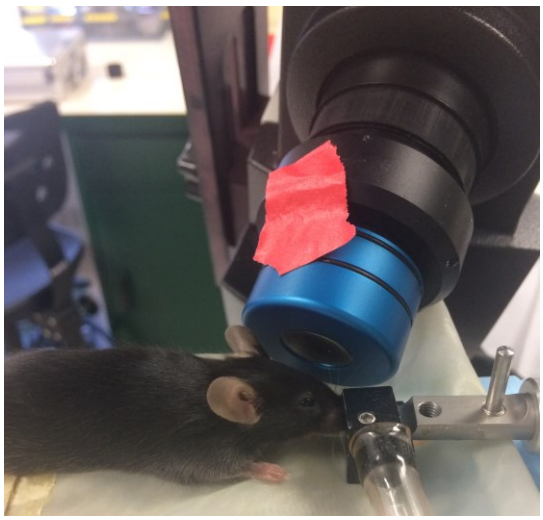

Figure 2-2. Mouse OCT setup.

2.5.2. Scans

Circle scans (100-frame averaged, 1536 sampling points) centered on the optic nerve head were taken for each mouse at 12-degree, 18-degree and 24-degree eccentricities (Figure 2-3). The baseline scans were first acquired with infrared (820 nm) illumination and set as the reference. Follow-up scans (i.e. repeat scans on the same retinal area), using the image tracking software whenever possible, were taken for each measurement after the LIRD treatment. Registration with the OCT eye tracking software was not always possible in the subsequent follow-up scans

due to unclear ocular media and excessive eye rotation. In these cases, the scans were performed without the eye tracking registration.

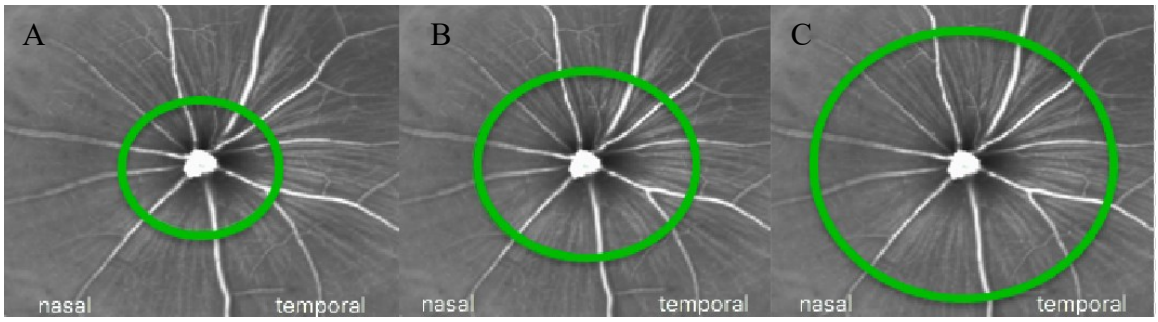

Figure 2-3. OCT circle scans of a C57BL/6 mouse acquired prior to LIRD treatment at (A) 12-degrees, (B) 18-degrees and (C) 24-degrees centered on the optic nerve head.

2.5.3. Data analysis

The OCT allows visualization of all the different layers of the retina, theoretically allowing quantification of each individual layer thickness and any subsequent loss after LIRD. It was qualitatively observed however that there were changes in the OCT reflectivity pattern in retinas that suffered changes from LIRD which made it difficult to determine the individual layers of the outer retina, and therefore we decided to quantify the inner and outer retinal thicknesses as a whole. The OCTs were manually segmented using Heidelberg Eye Explorer (Heidelberg Engineering GmbH) at the inner limiting membrane (ILM), inner plexiform layer (IPL) and retinal pigmented epithelium (RPE). The inner retina was measured from the ILM to the IPL, and the outer retina was measured from the IPL to the RPE (Figure 2-4). The segmentation data (1536 measurements per circle scan) was exported to a spreadsheet and used to calculate for the inner and outer retinal thicknesses by averaging per quadrant or over the entire retina.

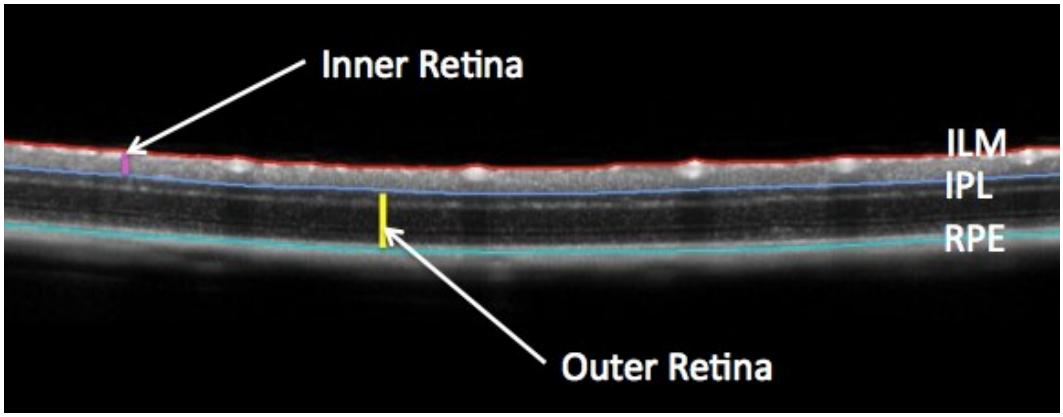

Figure 2-4. Segmentation of a 12-degree OCT circle scan of a C57BL/6 mouse acquired prior to LIRD treatment. The inner retina was measured from the ILM to the IPL, and the outer retina was measured from the IPL to the RPE.

2.6. Tissue harvest

Mice were sacrificed by lethal injection of 0.3mL pentobarbital sodium (Euthanyl, Bimeda-MTC Animal Health, Inc., Cambridge, ON, Canada). A suture (Vicryl 8.0, Eye Care and Cure, Tucson, AZ, USA) was made in the superior conjunctiva to indicate orientation, and the eyes were immediately enucleated and fixed overnight in 4% paraformaldehyde (diluted from 16% formaldehyde solution, 28908, Thermo Scientific, Rockford, IL, USA). Eyes were cryoprotected in 30% sucrose (Fisher Scientific, Fair Lawn, NJ, USA) and stored in a -80°C freezer if not immediately processed for histology or immunohistochemistry.

2.7. Retinal frozen sections for Rhodopsin labelling

Eyes were frozen in Tissue-Plus O.C.T compound (Fisher HealthCare, Houston, TX, USA) at -15°C and cut into 10-12µm sections (Leica CM 1850 cryostat, Leica Microsystems GmbH, Wetzlar, Germany) comprising both superior and inferior

portions of the retina. Rhodopsin labelling was performed to visualize the expression of rhodopsin in the outer segments and TO-PRO was used to visualize cell nuclei. Frozen sections were washed in phosphate buffered saline (PBS, diluted from 10X PBS, AM9625, Invitrogen, Waltham, MA, USA) for 10 min then incubated in a blocking buffer of 10% normal goat serum (005-000-121, Jackson ImmunoResearch Laboratories Inc., West Grove, PA, USA) and 0.3% Triton X-100 (Sigma-Aldrich) in PBS for 1 hr at room temperature followed by incubation with 1:500 primary antibody (Anti-rhodopsin antibody, MAB5356, EMD Millipore Corporation, Temecula, CA, USA) in blocking buffer overnight at 4°C. The sections were then washed 3×5-min with PBS and incubated in 1:500 anti-mouse secondary antibody conjugated to Cy 3 (115-165-003, Jackson ImmunoResearch Laboratories Inc.) for 1 hr at room temperature. The sections were washed again 3×5-min with PBS then incubated in 1:1000 TO-PRO-3 Iodide (T3605, Molecular Probes, Eugene, OR, USA). After a final wash of 3×5-min with PBS, sections were mounted using Vectashield (H-1000, Vector Laboratories, Burlingame, CA, USA) and imaged with Zeiss Axio Imager M2 microscope (Carl Zeiss AG).

2.7.1. Quantification of photoreceptors and outer segment length by labelling rhodopsin and cell nuclei (TO-PRO).

For each eye, photoreceptor cells in two areas (the superior retina and the inferior retina) were quantified by counting the rows of nuclei in the ONL (Figure 2-5) of 5 sections and averaged. Outer segment length was measured (Zen2Lite, Carl

Zeiss Meditec, Oberkochen, Germany) from 5 sections in two areas (superior and inferior retina) and averaged.

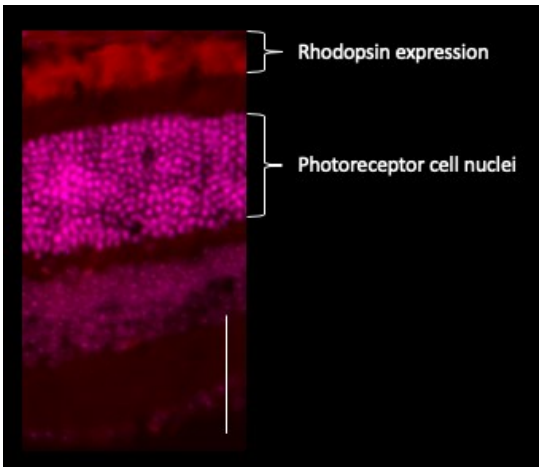

Figure 2-5. Retinal section from a C57/BL6 mouse labelled with rhodopsin (red) and TO-PRO for cell nuclei (pink). Scale bar = 50µm. Magnification = 20x.

2.8. Retinal flat mounts for retinal ganglion cell labelling

2.8.1. RNA binding protein with multiple splicing

RNA binding protein with multiple splicing (RBPMS), a selective marker for mammalian RGCs (Rodriguez et al., 2014), was used for RGC labelling. Retinas were first incubated in a blocking buffer of 10% normal goat serum and 0.5% Triton X-100 in PBS overnight at 4°C followed by incubation with 1:1000 primary antibody (Anti-RBPMS antibody, 1832-RBPMS, PhosphoSolutions, Aurora, CO, USA) and 0.5% Triton X-100 in PBS for 3-5 nights at 4°C. The sections were then washed 3×30-min with PBS and incubated with 1:500 anti-guinea pig secondary antibody conjugated to Cy 3 (706-165-148, Jackson ImmunoResearch Laboratories Inc.) overnight at 4°C. The sections were washed again 3×30-min with PBS and 4 shallow cuts were made so that the retina lies flat with 4 quadrants (superior, inferior, nasal and temporal).

The retinas were then mounted using Vectashield and imaged with Zeiss Axio Imager M2 microscope.

2.8.2. Quantification of retinal ganglion cells

Using Zen2Lite (Carl Zeiss Meditec), regions of interest (ROI) of 500 x 500 μm were selected from the central, middle and periphery in each of the four quadrants. The total number of labeled cells was counted for each ROI and divided by the retinal area to calculate the RGC density (cells/mm^2). Cell densities were grouped by retinal eccentricities and averaged for each retina.

2.9. Sample size calculations

To determine if there was a sufficient number of pigmented and albino mice used for this project, post hoc sample size calculations (ANOVA: repeated measures, within factors) were made using the existing data (from Baseline up to approximately Day 28) with G*Power (Faul, et al., 2007; Faul et al., 2009) for the pSTR (brightest flash stimuli: -3.2 log cd s/m^2) and a-wave (brightest flash stimuli: 1.0 log cd s/m^2) ERGs. The partial eta squared and correlation among repeated measures (Pearson correlation coefficient) was calculated with SPSS Statistics (Version 24, IBM Corp., Armonk, NY, USA), which was then inputted into G*Power for the calculations. Because the number of animals used already exceeded the sample sizes calculated, no further animals were used for the study. Table 2-1 lists the parameters used for sample size calculations using an α error probability of 0.05 and a power (1-β) of 0.8.

Table 2-1. Sample sizes calculated using pSTR and a-wave data for pigmented and albino mice

		Effect size	Correlation among repeated measures	Sample size calculated
Pigmented mice	**pSTR**	2.17	-0.290	2
	a-wave	3.62	0.826	2
Albino mice	**pSTR**	1.80	0.289	2
	a-wave	2.71	0.870	2

2.10. Statistical Analyses

Retinal thickness was calculated, and then retinal thickness and ERG amplitudes were normalized to percent from baseline (Microsoft Excel 2011, Microsoft Corporation, Redmond, WA). The data were then exported to software (Prism, Version 8, Graphpad Software, San Diego, CA; or SPSS, Version 24, IBM Corp., Armonk, NY, USA) for statistical analyses. Linear regression analyses were performed to assess decreasing trends of OCT (outer and inner retinal thickness) and ERG (a-wave, b-wave, pSTR and nSTR amplitudes) results. ANOVA tests were performed to examine main effects of strain, retinal eccentricity and retinal quadrant. Correlation analyses were used to examine relationships between ERG waveforms, and between ERG waveforms and retinal thickness.

3. Chapter 3: Results

A total of 10 pigmented C57BL/6 mice and 6 albino BALB/c mice were used for the LIRD experiments. The number of eyes and observations for each time-point are shown in Appendix A and B. 6 pigmented and 4 albino naïve mice were used as controls for immunohistological analyses. In addition, 6 pigmented mice were used for preliminary experiments (discussed in Section 4.1) to establish the LIRD protocol and a further 10-20 mice with different genetic backgrounds were used for ERG training and immunohistochemistry practice.

3.1. Structural changes in the retina after LIRD in pigmented mice

In pigmented mice, there was no loss of inner or outer retinal thickness evident in the OCT images (Figure 3-1) and retinal thickness plots (Figure 3-2) over a 117-day period after LIRD. Linear regression analysis of the average retinal thickness over the entire length of the retina showed no significant decrease in outer retinal thickness at 12 degree ($p=0.14$, $R^2=0.03$), 18 degree ($p=0.30$, $R^2= 0.02$) or 24 degree ($p=0.01$, $R^2<0.01$) eccentricities (Figure 3-3 A-C). Similarly, there was no significant decrease of the average inner retinal thickness at 12 degrees ($p=0.10$, $R^2=0.04$), 18 degrees ($p=0.49$, $R^2=0.01$) or 24 degrees ($p=0.12$, $R^2=0.03$) from the optic nerve head (Figure 3-3 D-F). Retinal thicknesses were examined with ANOVA for each of the retinal quadrants nasal, superior, temporal and inferior to see if there were any differences in retinal loss based on quadrant location in the retina. There was a significant effect of retinal quadrant at the 12 degree eccentricity ($p=0.02$) in

the outer retina, but not at the 18 degree (p=0.40) or 24 degree (p=0.07) eccentricities (Figure 3-4 A-C). There was a significant effect of retinal quadrant at the 12 and 18 degree eccentricities (p=0.02 for 12 degrees; p=0.03 for 18 degrees) but not the 24 degree eccentricity (p=0.07) in the inner retina Figure 3-4 D-F).

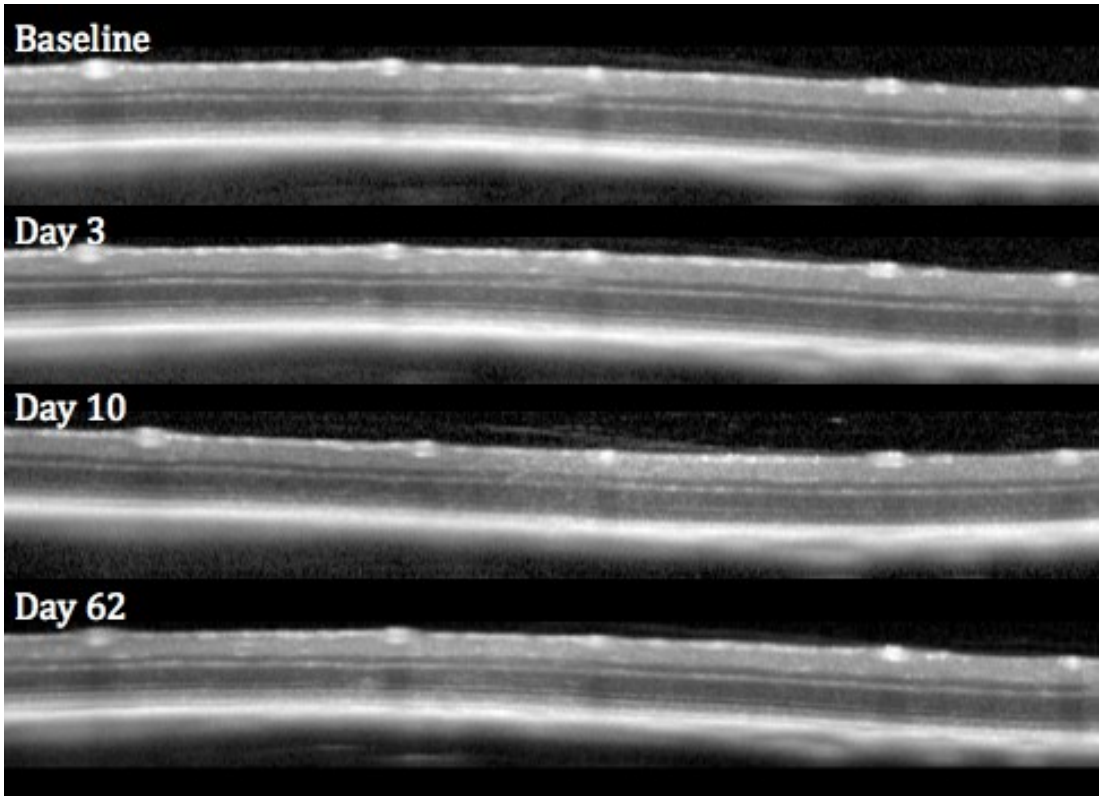

Figure 3-1. OCT scans of one representative pigmented mouse 18 degrees from the optic nerve head.

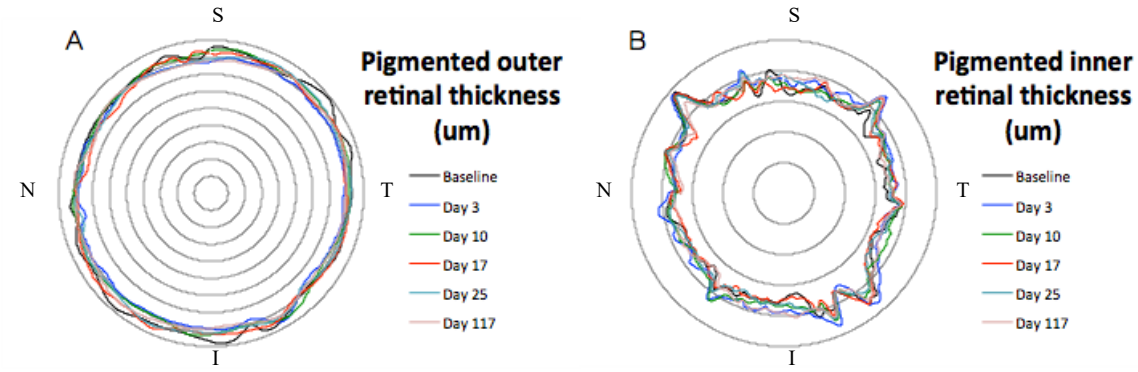

Figure 3-2. Polar retinal thickness plot of the (A) outer and (B) inner retina of one representative pigmented mouse at 18 degrees from the optic nerve head. Each concentric ring represents 20 µm. N = nasal, S = superior, T = temporal, I = inferior.

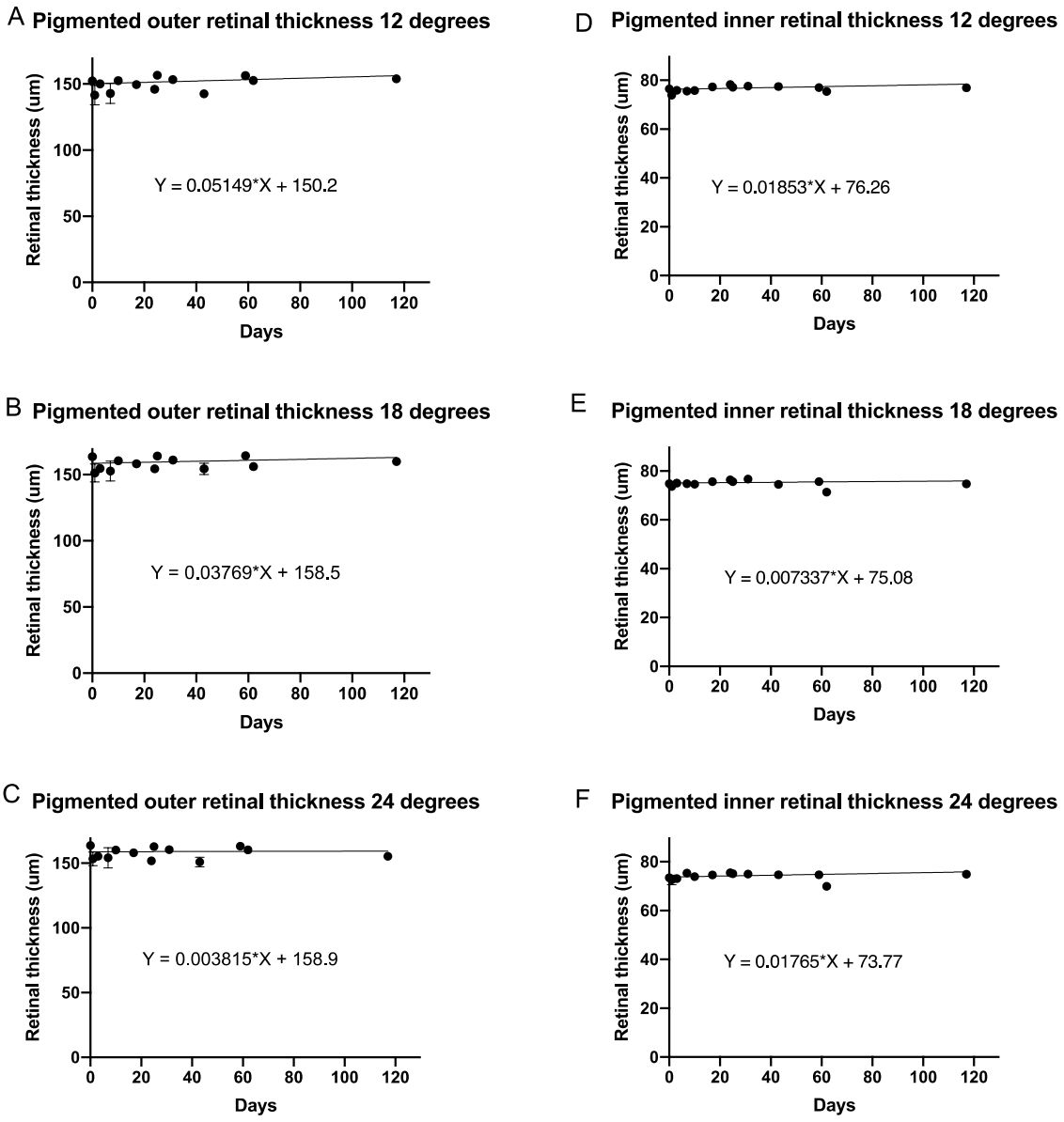

Figure 3-3. In pigmented mice, linear regression analysis did not show a decrease in outer retinal thickness after LIRD at (A) 12 degrees, (B) 18 degrees and (C) 24 degrees from the optic nerve head. Similarly, there was no decrease in inner retinal thickness at 12, 18 and 24 degree eccentricities in the inner retina (D-F). Error bars denote SEM.

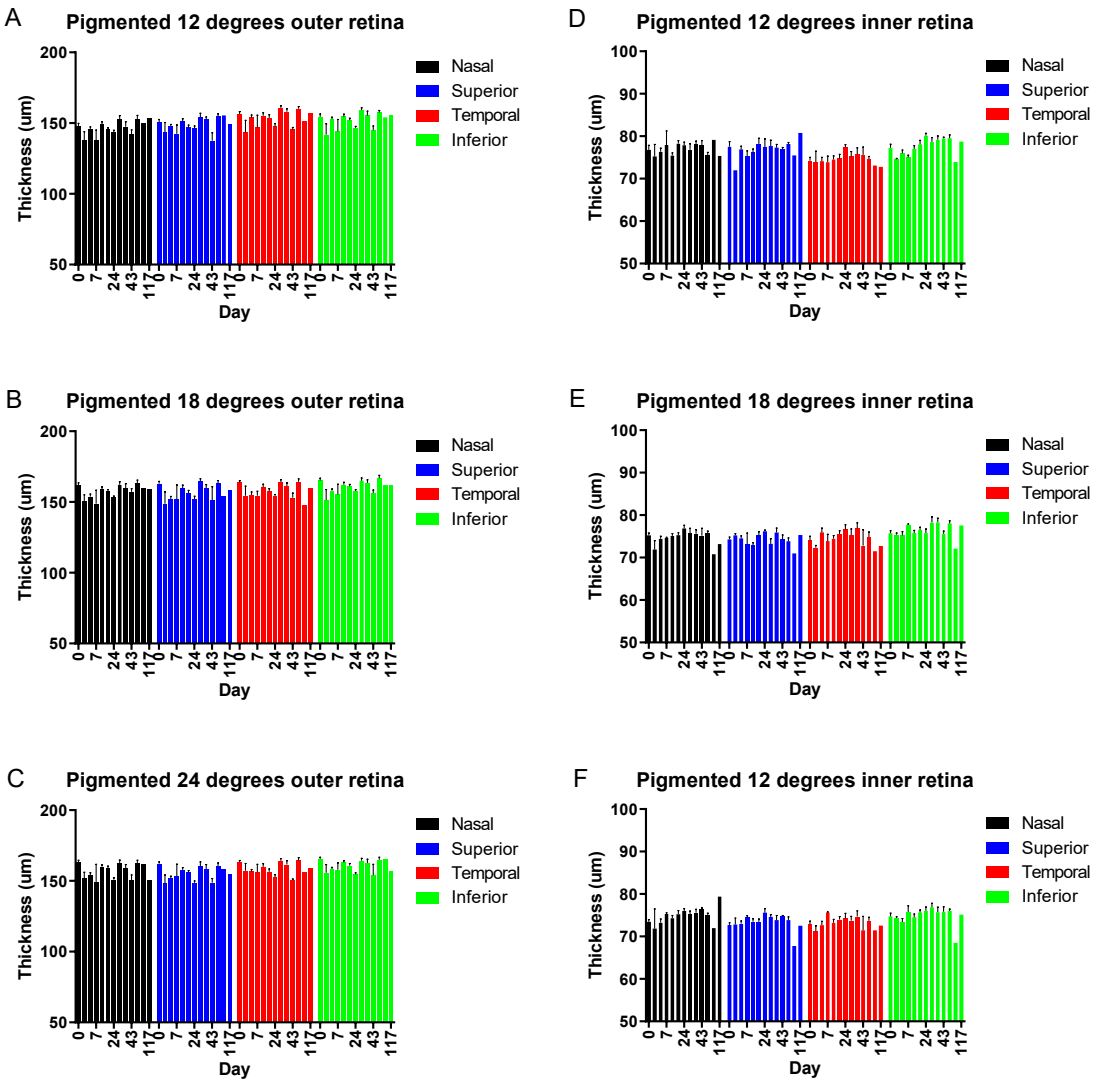

Figure 3-4. Mean outer retinal thickness (A-C) and inner retinal thickness (D-F) for the nasal, superior, inferior and temporal quadrants over time at 12, 18 and 24 degrees from the optic nerve head in pigmented mice. Error bars denote SEM.

3.2. Functional changes in the retina after LIRD in pigmented mice

Functionally, LIRD caused a decrease in ERG amplitude in all of the waveforms in pigmented mice (Figure 3-5). The mean ERG amplitudes decreased until Day 14 and afterward remained stable up to Day 121. The amplitudes for each ERG waveform were normalized to percent from baseline to account for individual variations. Two

specific light intensities (one dimmer and one brighter) were chosen to be examined more closely from the range of light intensities used for the STRs as well as the a- and b-waves. For the a- and b-waves, the light intensities -1.2 and 1.0 log cd s m^{-2} were examined. -1.2 log cd s m^{-2} is the dimmest flash intensity where the a-wave starts to appear (See Fig 3-5 A) and 1.0 log cd s m^{-2} is the maximum brightest flash intensity. For the pSTR and nSTR, the light intensities -4.8 and -3.2 log cd s m^{-2} were examined. -4.8 log cd s m^{-2} is the flash intensity where the minimum pSTR and nSTR amplitude was obtained (Figure 3-5 E-F). The STR amplitudes were not smaller at the next dimmest flash intensity. Except for the nSTR at -4.8 log cd s m^{-2}, all other ERGs examined showed an overall decreasing trend of ERG amplitude after LIRD (Table 3-2, Figure 3-6).

Table 3-1. Linear regression analysis of ERG amplitudes of pigmented mice after LIRD. Data normalized to percent from baseline. Significance is indicated in bold.

Light intensity	Equation	p	R^2
a-wave			
-1.2 log cd s m^{-2}	Y = -0.4924*X + 85.71	**<0.01**	0.25
1.0 log cd s m^{-2}	Y = -0.3237*X + 88.09	**<0.01**	0.29
b-wave			
-1.2 log cd s m^{-2}	Y = -0.3089*X + 86.21	**<0.01**	0.19
1.0 log cd s m^{-2}	Y = -0.3375*X + 86.93	**<0.01**	0.26
pSTR			
-4.8 log cd s m^{-2}	Y = -0.4030*X + 111.3	**0.03**	0.04
-3.2 log cd s m^{-2}	Y = -0.4486*X + 93.58	**<0.01**	0.25
nSTR			
-4.8 log cd s m^{-2}	Y = 0.1272*X + 122.7	0.69	<0.01
-3.2 log cd s m^{-2}	Y = -0.2457*X + 92.88	**0.02**	0.05

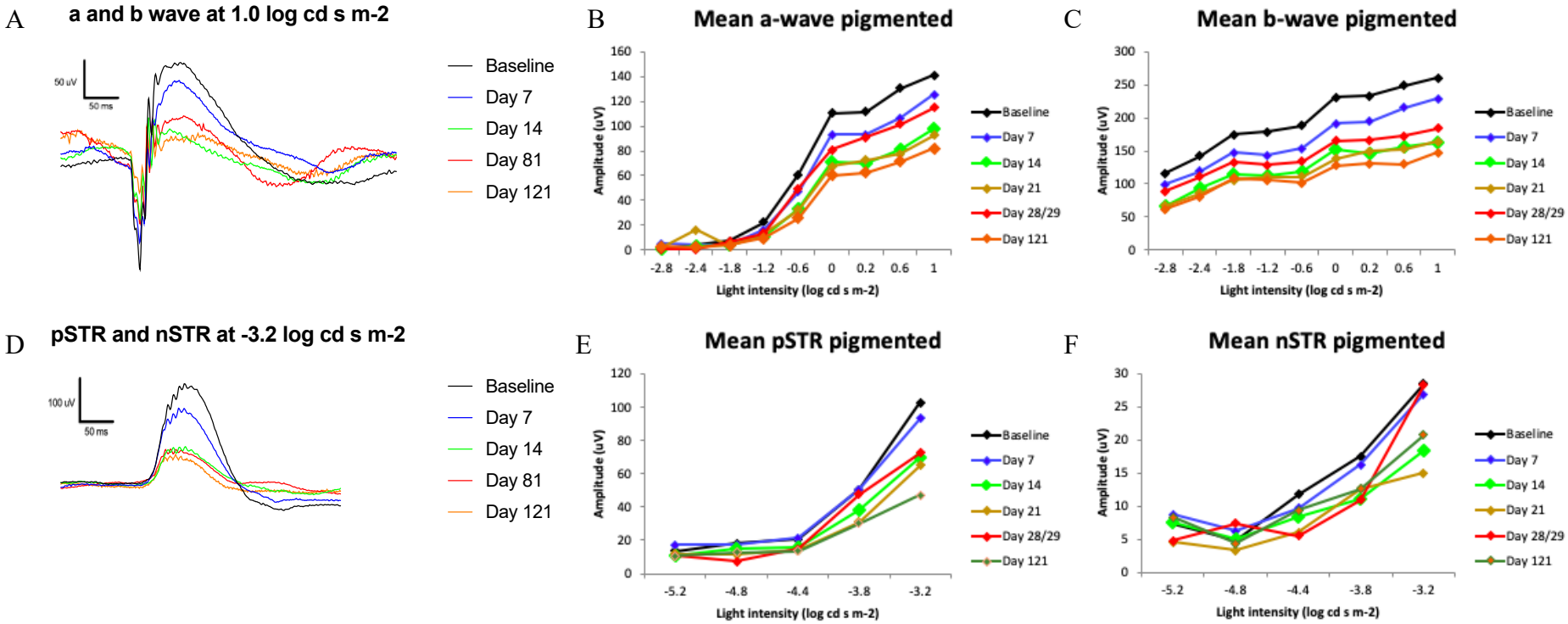

Figure 3-5. LIRD caused a decrease in all ERG amplitudes in pigmented mice. At a bright light intensity (1.0 log cd s m^{-2}), (A) demonstrates how the a and b waveforms decreased after LIRD compared to baseline in one representative animal. (B-C) show how the mean a-wave and b-wave amplitudes, plotted over increasing light intensity, change after LIRD. At a dim light intensity (-3.2 log cd s m^{-2}), (D) demonstrates how the pSTR and nSTR decreased after LIRD compared to baseline. (B-C) show how the mean pSTR and nSTR amplitudes, plotted over increasing light intensity, change after LIRD.

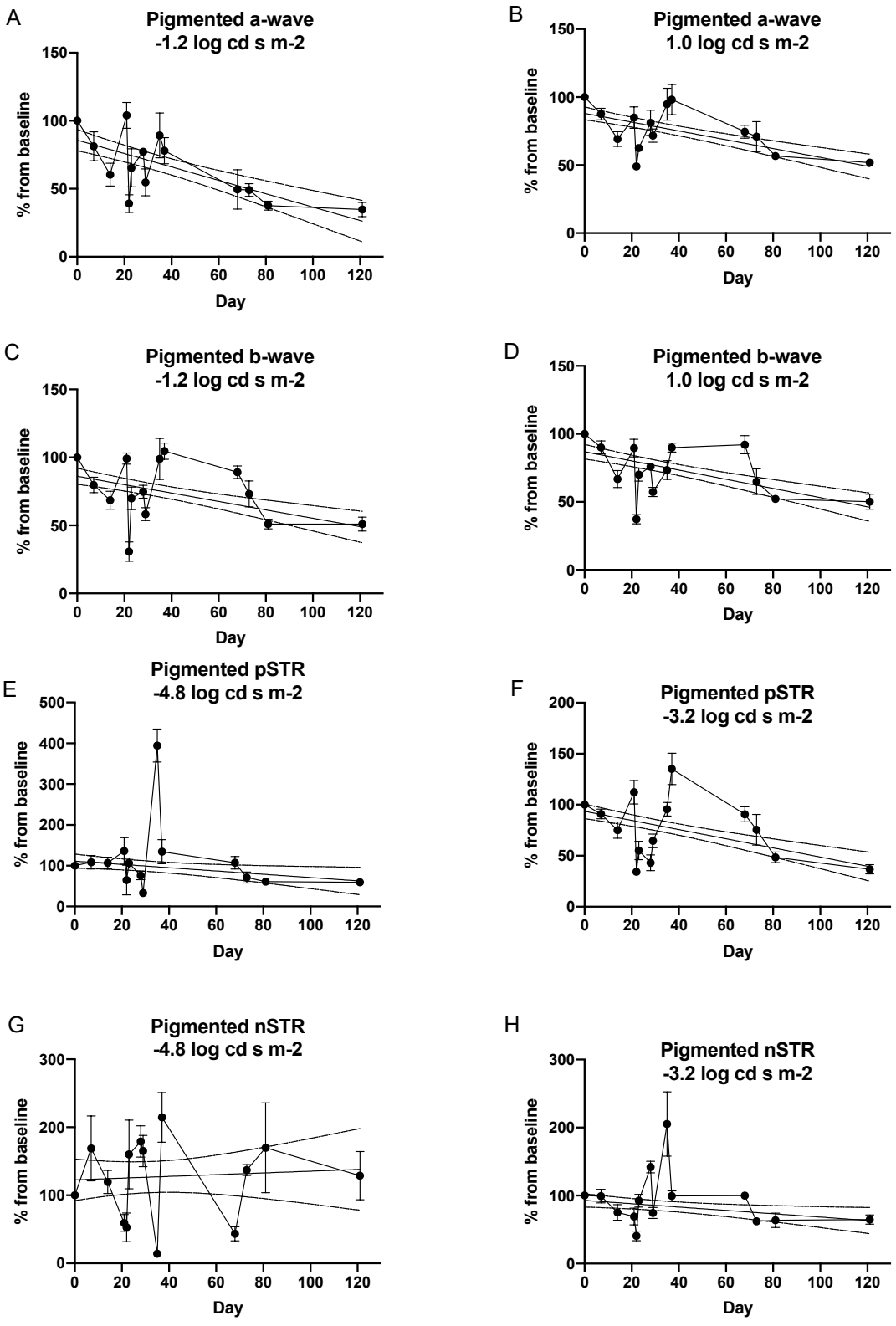

Figure 3-6. Changes in (A) a-wave, (B) b-wave, (C) pSTR and (D) nSTR amplitudes over time after LIRD in pigmented mice. Data normalized to percent from baseline. Error bars denote SEM. 95% confidence interval band of best-fit line included.

3.3. Structural changes in the retina after LIRD in albino mice

Because retinal thickness loss was not observed after LIRD in pigmented mice, we decided to perform the same experiment in albino mice, which are known to show outer retinal thickness loss after LIRD (Wasowicz et al., 2002; Bhavna et al., 2017). In these mice, subjective assessment of both OCT scans (Figure 3-7) and retinal thickness plots (Figure 3-8) show apparent thickness loss in the outer retina over a 62 day period. Subjective examination of the outer retinal thickness plots (Figure 3-8 A) show that outer retinal thickness seems to decrease up to Day 10 post-LIRD, and then remains stable after that. There was no obvious loss in inner retinal thickness.

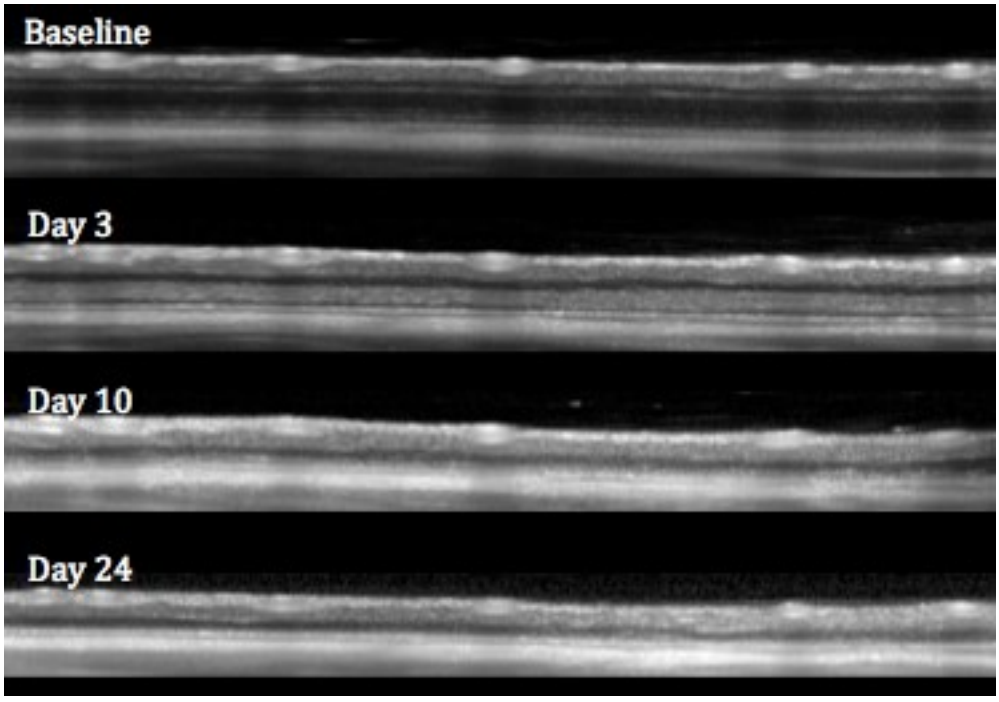

Figure 3-7. OCT scans of one representative albino mouse 18 degrees from the optic nerve head.

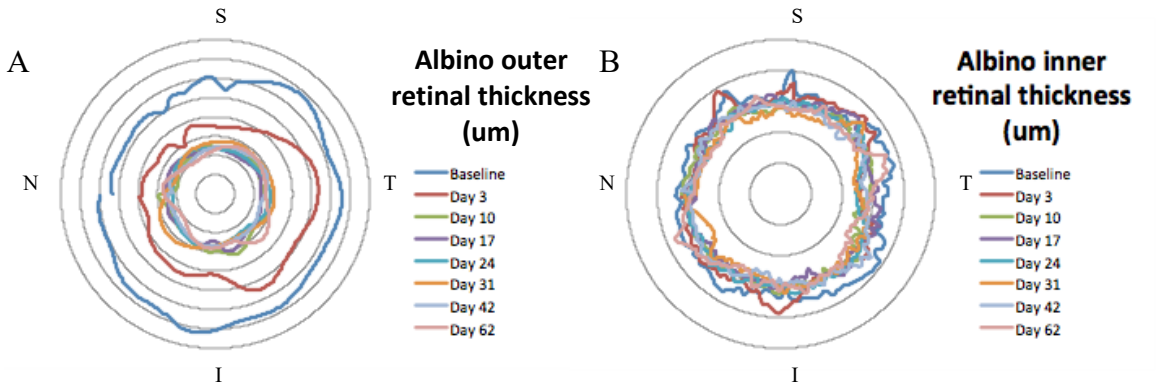

Figure 3-8. Polar retinal thickness plot of the (A) outer and (B) inner retina of one representative albino mouse at 18 degrees from the optic nerve head. Each concentric ring represents 20μm of retinal thickness. N = nasal, S = superior, T = temporal, I = inferior.

In the outer retina, because the data points appear to have a sharp decrease in thickness during the acute early time points post-LIRD followed by what appears to be a plateau, they were fitted with two linear regression lines (Figure 3-9 A-C). Regression lines were split between Day 0-10 and post-Day 10 in agreement with what was observed in the outer retinal thickness plots (Figure 3-8 A). Analyses showed a significant decrease in the early acute phase ($p<0.01$, $R^2=0.76$ for 12 degrees; $p<0.01$, $R^2=0.73$ for 18 degrees; $p<0.01$, $R^2=0.66$ for 24 degrees) in all eccentricities. No significant decrease was found in the later phase post-Day 10 ($p=0.30$, $R^2=0.06$ for 12 degrees; $p=0.42$, $R^2=0.04$ for 18 degrees; $p=0.58$, $R^2=0.02$ for 24 degrees; Figure 3-9 A-C). The inner retinal thickness data points were fitted with a single linear regression, and showed significant decrease at all ecccentricities ($p=0.01$, $R^2=0.12$ for 12 degrees; $p<0.01$, $R^2=0.33$ for 18 degrees; $p<0.01$, $R^2=0.39$ for 24 degrees Figure 3-9 D-F). ANOVA tests show no significant effect of quadrant at all eccentricities ($p=0.17$ for 12 degrees; $p=0.18$ for 18 degrees; $p=0.29$ for 24 degrees)

in the outer retina. Similarly there was no significant effect of retinal quadrant at all eccentricities (p=0.49 for 12 degrees; p=0.20 for 18 degrees; p=0.10 for 24 degrees) in the inner retina.

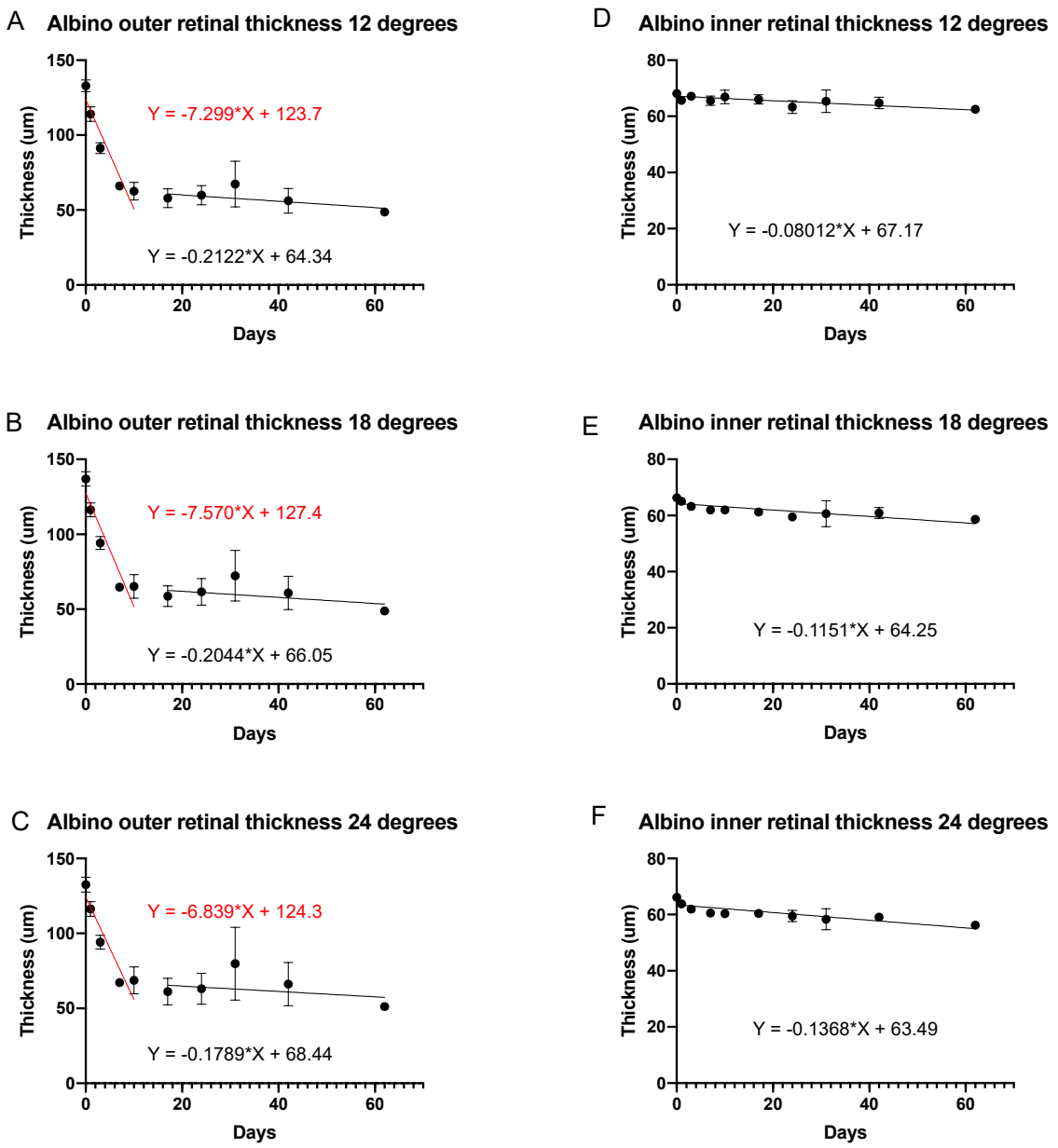

Figure 3-9. In albino mice, linear regression analysis showed a significant decrease in outer retinal thickness after LIRD at (A) 12 degrees, (B) 18 degrees and (C) 24 degrees from the optic nerve head. Similarly, there was a significant decrease in inner retinal thickness at 12, 18 and 24 degree eccentricities in the inner retina (D-F). Error bars denote SEM.

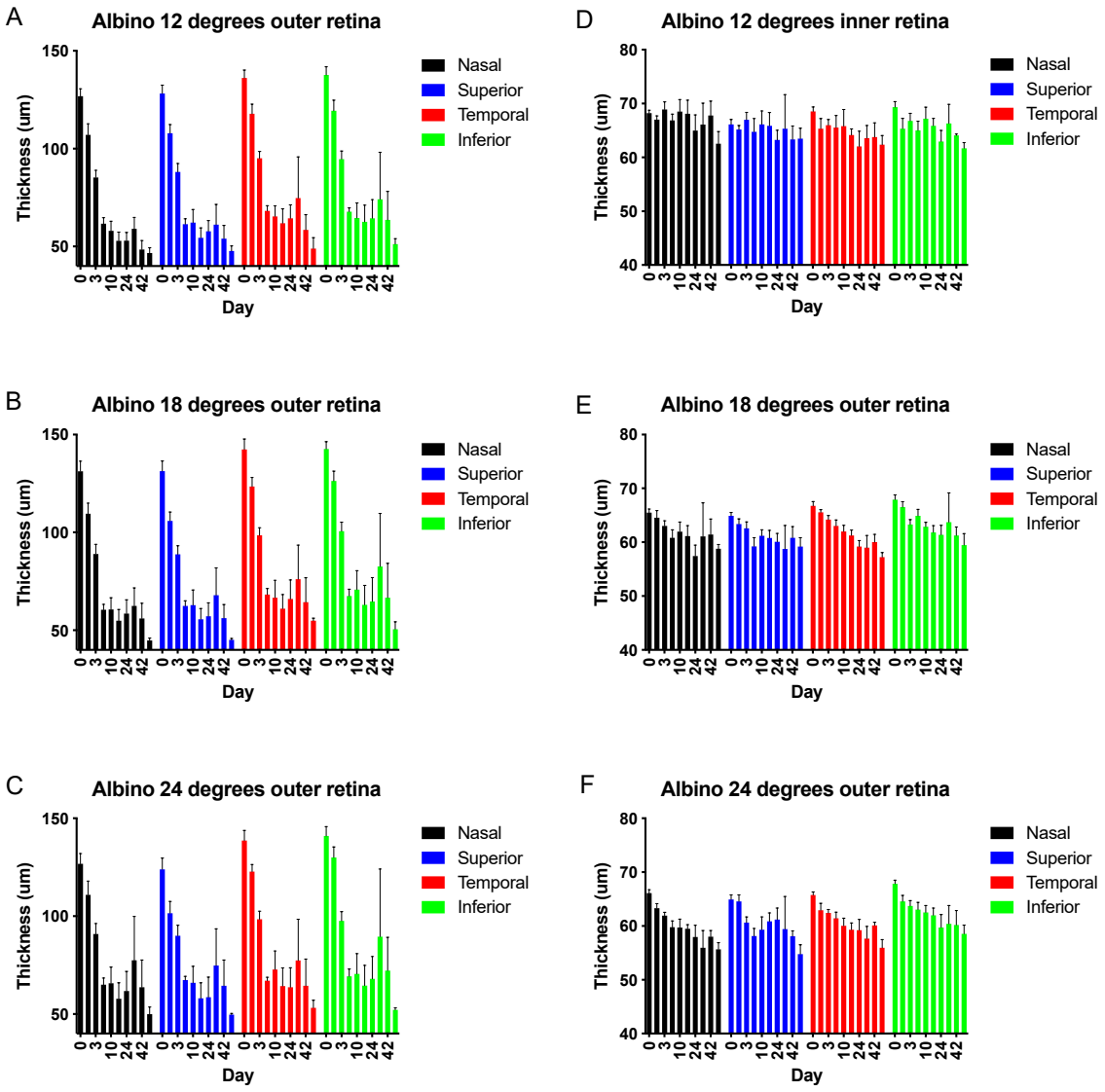

Figure 3-10. Mean outer retinal thickness (A-C) and inner retinal thickness (D-F) for the nasal, superior, inferior and temporal quadrants over time at 12, 18 and 24 degrees from the optic nerve head in albino mice. Error bars denote SEM.

3.4. Functional changes in the retina after LIRD in albino mice

Functionally, LIRD caused a decrease in ERG amplitude in all of the waveforms in albino mice (Figure 3-11). Mean ERG amplitudes appeared to decrease until Day 7 and remain approximately stable up to Day 62. Linear regression of the normalized ERG amplitudes after LIRD were examined at the light intensities -1.2 and 1.0 log cd s m^{-2} for a- and b-waves, and -4.8 and -3.2 log cd s m^{-2} (Table 3-4, Figure 3-12).

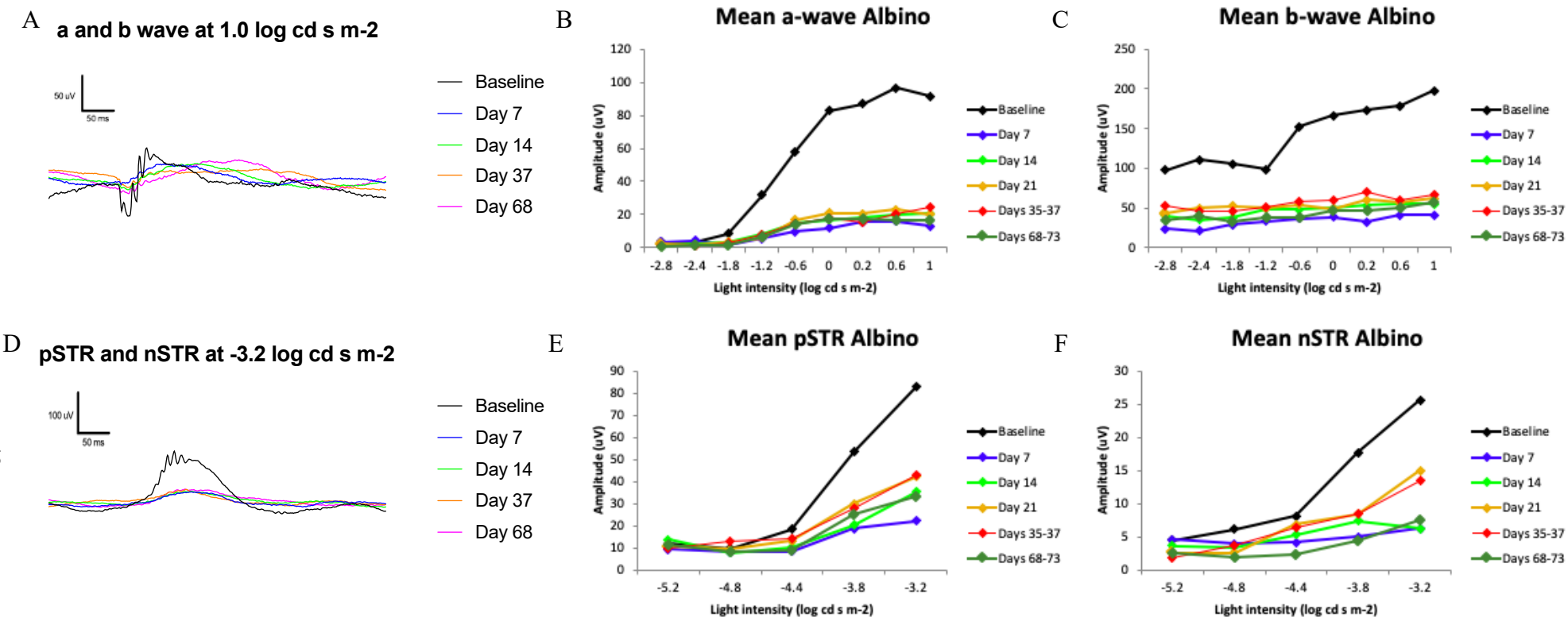

Figure 3-11. LIRD caused a decrease in all ERG amplitudes in albino mice. At a bright light intensity (1.0 log cd s m^{-2}), (A) demonstrates how the a and b waveforms decreased after LIRD compared to baseline in one representative animal. (B-C) show how the mean a-wave and b-wave amplitudes, plotted over increasing light intensity, change after LIRD. At a dim light intensity (-3.2 log cd s m^{-2}), (D) demonstrate how the pSTR and nSTR decreased after LIRD compared to baseline. (B-C) show how the mean pSTR and nSTR amplitudes, plotted over increasing light intensity, change after LIRD.

Table 3-2. Linear regression analysis of ERG amplitudes of albino mice after LIRD. Data normalized to percent from baseline. Significance is indicated in bold.

Light intensity	Equation	p	R^2
a-wave			
-1.2 log cd s m^{-2}	Y = -0.5646*X + 51.42	**0.01**	0.10
1.0 log cd s m^{-2}	Y = -0.6547*X + 47.27	**<0.01**	0.16
b-wave			
-1.2 log cd s m^{-2}	Y = -0.3390*X + 65.50	0.14	0.04
1.0 log cd s m^{-2}	Y = -0.5305*X + 52.21	**<0.01**	0.12
pSTR			
-4.8 log cd s m^{-2}	Y = 0.1680*X + 108.0	**0.03**	0.04
-3.2 log cd s m^{-2}	Y = -0.2491*X + 60.50	**<0.01**	0.25
nSTR			
-4.8 log cd s m^{-2}	Y = -0.6157*X + 79.03	**0.01**	0.10
-3.2 log cd s m^{-2}	Y = -0.4288*X + 59.52	**0.05**	0.06

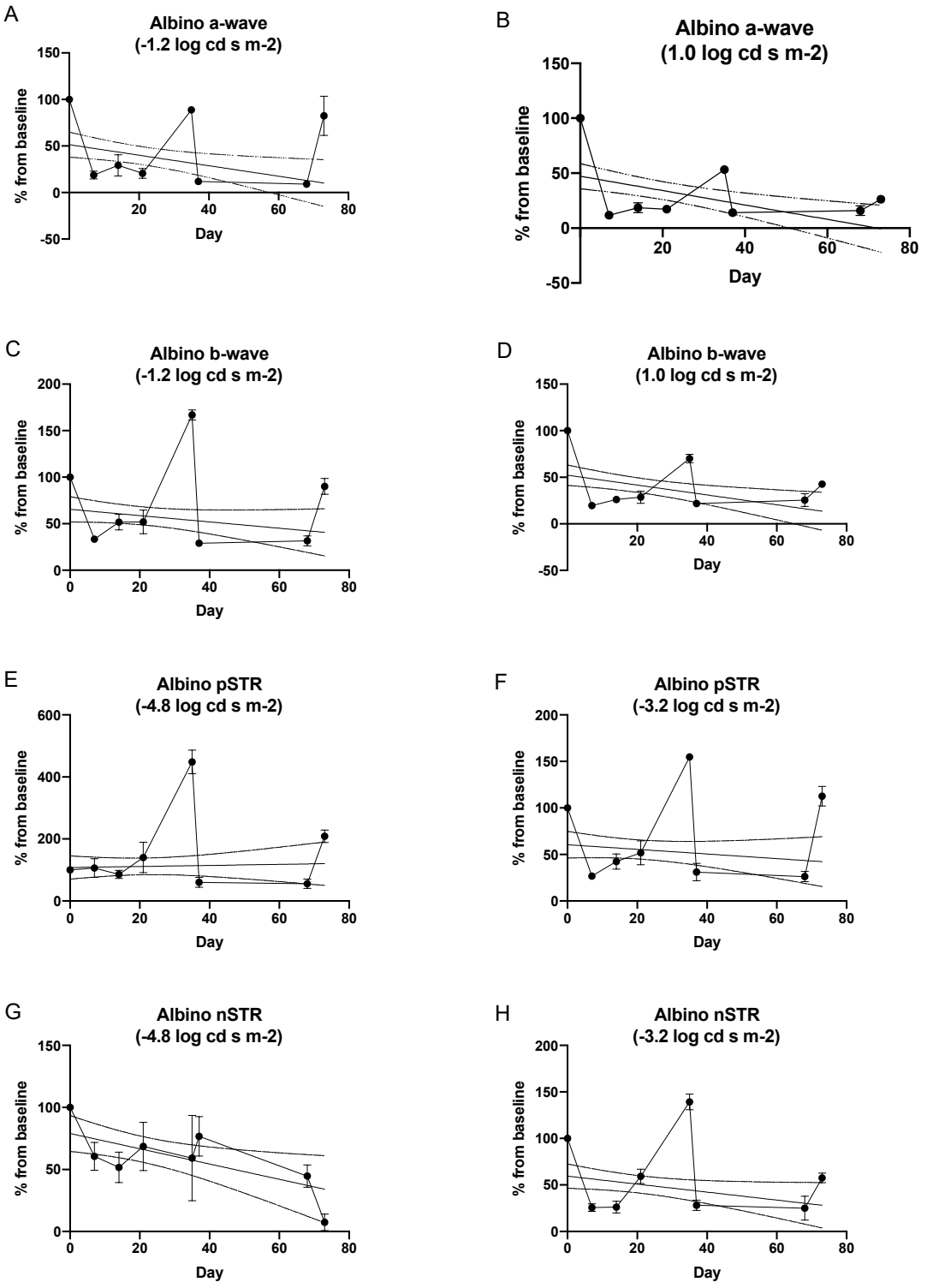

Figure 3-12 Changes in (A) a-wave, (B) b-wave, (C) pSTR and (D) nSTR amplitudes over time after LIRD in albino mice. Data normalized to percent from baseline. Error bars denote SEM. 95% confidence interval band of best-fit line included.

3.5. Strain differences in structural and functional changes after LIRD

ANOVA tests of outer retinal thickness showed a significant main effect of strain ($p<0.01$) but no significant effect of retinal eccentricity ($p=0.06$). Inner retinal thickness showed a significant main effect of strain ($p<0.01$) and retinal eccentricity ($p<0.01$). ANOVA tests showed a significant effect ($p<0.01$) of mouse strain on a- and b-wave amplitudes examined at flash intensities -1.2 and 1.0 log cd s m-2. The effect of mouse strain was not significant for pSTR at -4.8 log cd s m-2 ($p=0.47$), but it was significant for pSTR at -3.2 log cd s m-2 as well as for nSTR at -4.8 and -3.2 log cd s m-2.

3.6. Correlation between ERG and retinal thickness

Normalized (% from baseline) ERG (at light intensities -3.2 and 1.0 log cd s m^{-2}) and retinal thickness data were compared. In pigmented mice, there was a significant correlation between the a-wave and b-wave (Pearson $r=0.74$, $p<0.01$), between the a-wave and pSTR (Pearson $r=0.75$, $p<0.01$) and between the a-wave and nSTR (Pearson $r=0.40$, $p<0.01$) (Figure 3-13 A-C). In albino mice, there was a significant correlation between the a-wave and b-wave (Pearson $r=0.97$, $p<0.01$), a-wave and pSTR (Pearson $r=0.74$, $p<0.01$), and a-wave and nSTR (Pearson $r=0.77$, $p<0.01$) (Figure 3-13 D-F).

Figure 3-13 shows the relationship between ERG waveforms. A line with a slope of one (blue dashed line) was overlaid over each graph to depict how a decrease in the a-wave amplitudes compares to the decrease in b-wave, pSTR or nSTR amplitudes. Individual data points falling above the blue line were interpreted

to mean less loss of pSTR or nSTR compared to loss of a-wave (See Discussion Section 4.3). Linear regression analyses were also performed and the slopes and intercepts (Table 3-3) were compared to see if there was a difference between comparisons. In pigmented mice, the slopes of the linear regression lines comparing a-wave vs. b-wave was significantly different from the slope comparing a-wave vs. pSTR ($p=0.02$). Due to the large difference between slopes, it was not possible to test the difference between intercepts with the statistical software. Figure 3-14 provides another way to examine differences between the linear relationships of ERG waveforms. The residuals of the ERG comparisons were plotted against a line with a slope of 1. The residuals of the a-wave vs. b-wave comparison appear to be normally distributed above and below the line, suggesting a good fit for a perfect linear relationship (Figure 3-14 A). The residuals of the a-wave vs. pSTR comparison appear normally distributed as well, although there may be slightly more data points that are skewed positively (Figure 3-14 B). There was no difference in the slope comparing a-wave vs. b-wave to the slope comparing a-wave vs. nSTR ($p=0.55$), but there was a significant difference in their intercepts ($p=0.01$) and is in agreement with the residual plot (Figure 3-14 C).

In albino mice, there was no significant difference between the slopes of the linear regression lines comparing a-wave vs. b-wave to a-wave vs pSTR ($p=0.68$), but there was a significant difference between their intercepts ($p<0.01$). The residual plot of the a-wave vs. b-wave comparison appear to be positively skewed, although the data points fit closely to the slope of 1 line (Within 20-30%; Figure 3-14 D). The residual plot of a-wave vs. pSTR comparison is positively skewed (more

than the a-wave vs. b-wave residual plot; Figure 3-14 E), agreeing with the difference between intercepts. There was no difference between the slopes comparing a-wave vs b-wave to a-wave vs nSTR (p=0.41) but there was a significant difference between their intercepts (p<0.01), which agrees with the residual plot (Figure 3-14 F).

Table 3-3. Linear regression equations for ERG comparisons in pigmented and albino mice

ERG waveforms compared	Linear regression equation
Pigmented mice	
a-wave compared to b-wave	Y = 0.8196*X +12.34
a-wave compared to pSTR	Y = 1.123*X - 7.549
a-wave compared to nSTR	Y = 0.7168*X + 29.68
Albino mice	
a-wave compared to b-wave	Y = 0.9025*X + 10.83
a-wave compared to pSTR	Y = 0.8594*X + 26.49
a-wave compared to nSTR	Y = 0.8241*X + 22.91

Comparison of retinal thickness with ERG waves show that in pigmented mice, there was no significant correlation between the outer retina and the a-wave (Pearson r=0.19, p=0.19), and between the outer retina and the b-wave (Pearson r=-0.19, p=0.18) (Figure 3-15 A-B). There was no significant correlation between the inner retina and pSTR (Pearson r=-0.26, p=0.06), however there was a significant negative correlation between the inner retina and the nSTR (Pearson r=-0.29, p=0.04) in pigmented mice (Figure 3-15 C-D). In albino mice, there was a significant positive correlation between the outer retina and the a-wave (Pearson r=0.96,

$p<0.01$), the outer retina and the b-wave (Pearson $r=0.94$, $p<0.01$), the inner retina and pSTR (Pearson $r=0.62$, $p<0.01$), and the inner retina and nSTR (Pearson $r=0.59$, $p<0.01$) (Figure 3-15 E-H).

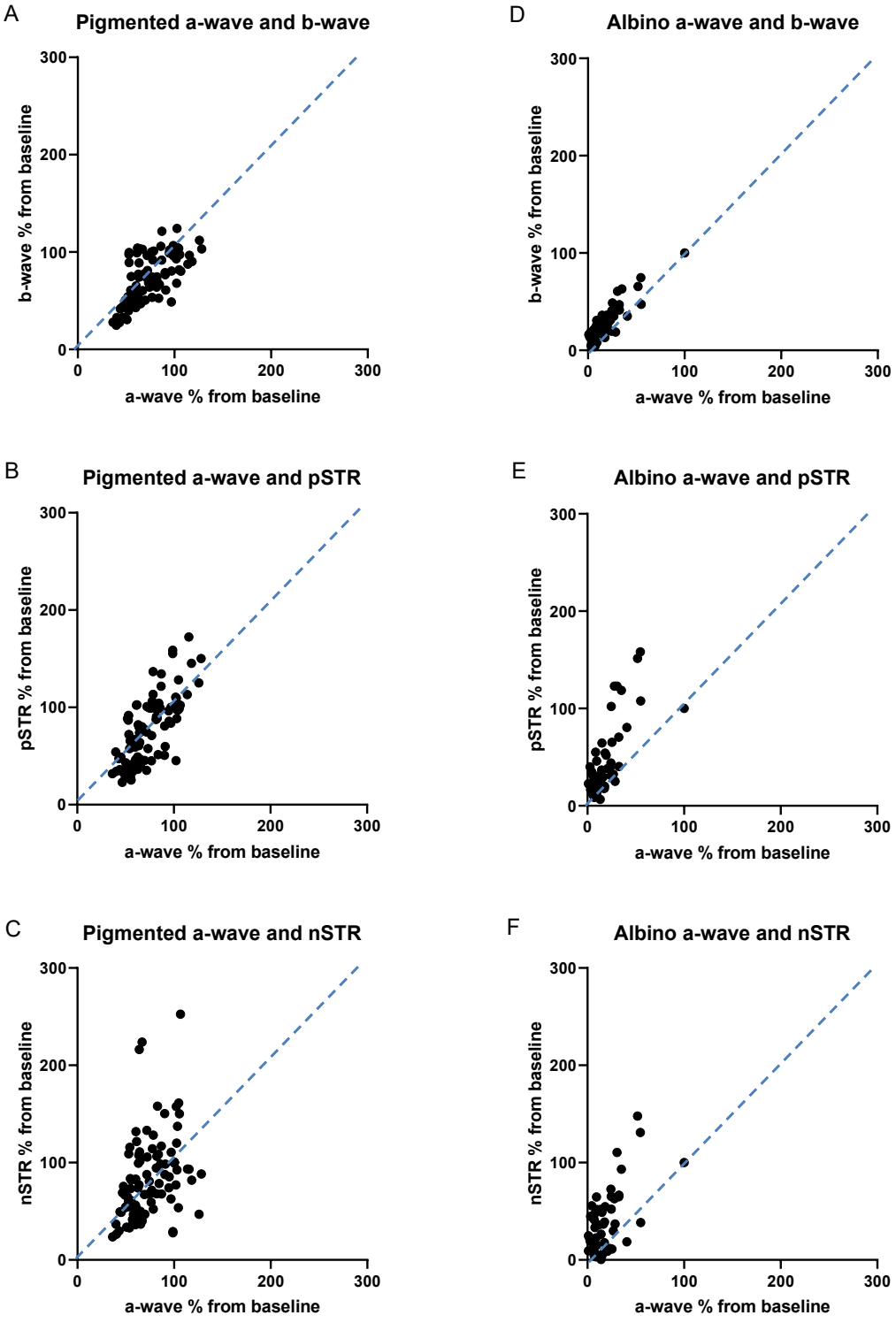

Figure 3-13. Correlation between normalized ERG waves for pigmented (A-C) and albino (D-F) mice. Individual data points are normalized to percent from baseline. The blue dashed lines indicate a slope of 1. Data points appearing above the line indicate less loss of pSTR or nSTR amplitude compared to loss of a-wave amplitude

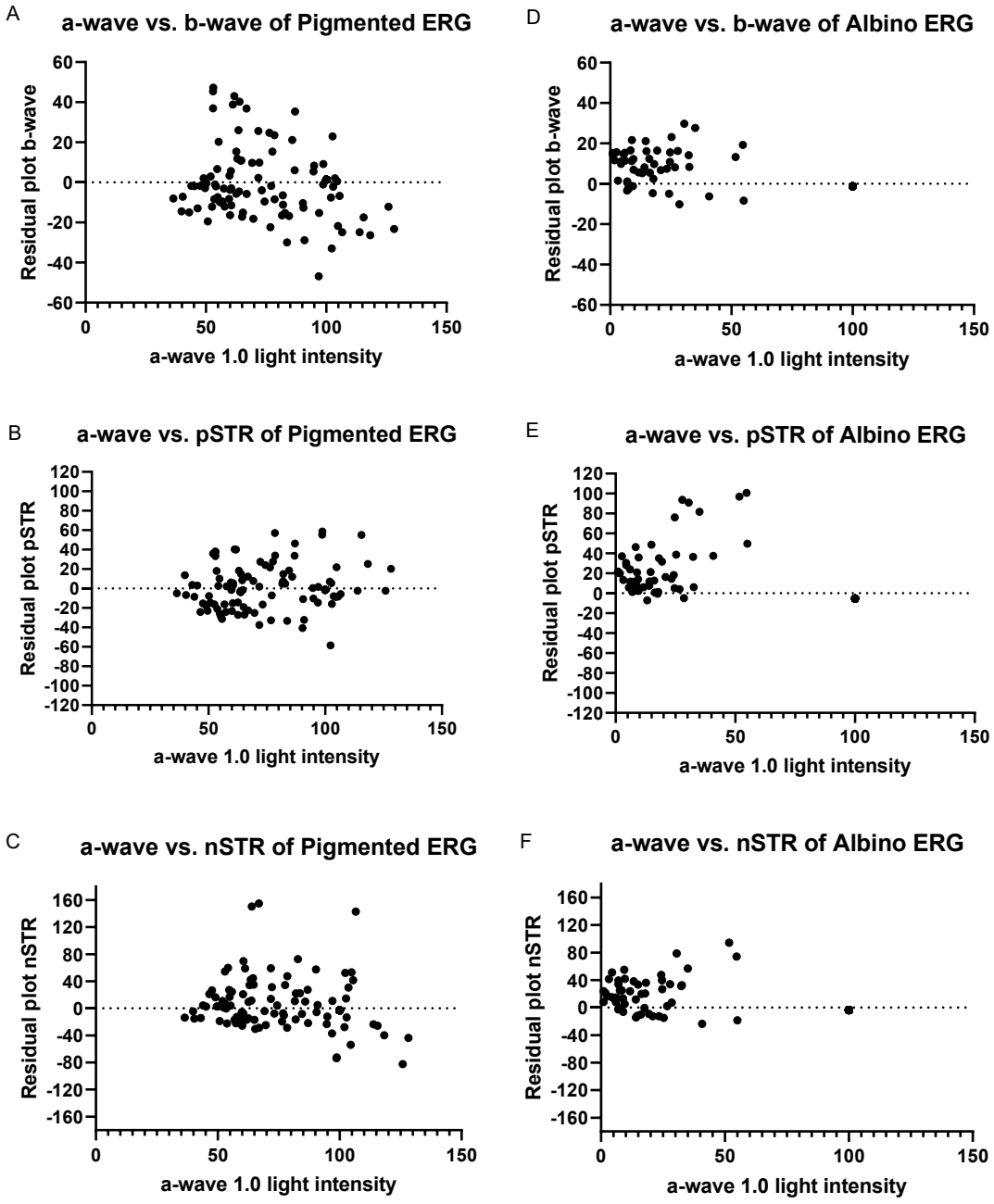

Figure 3-14. Residual plots of ERG comparisons against a slope of 1.

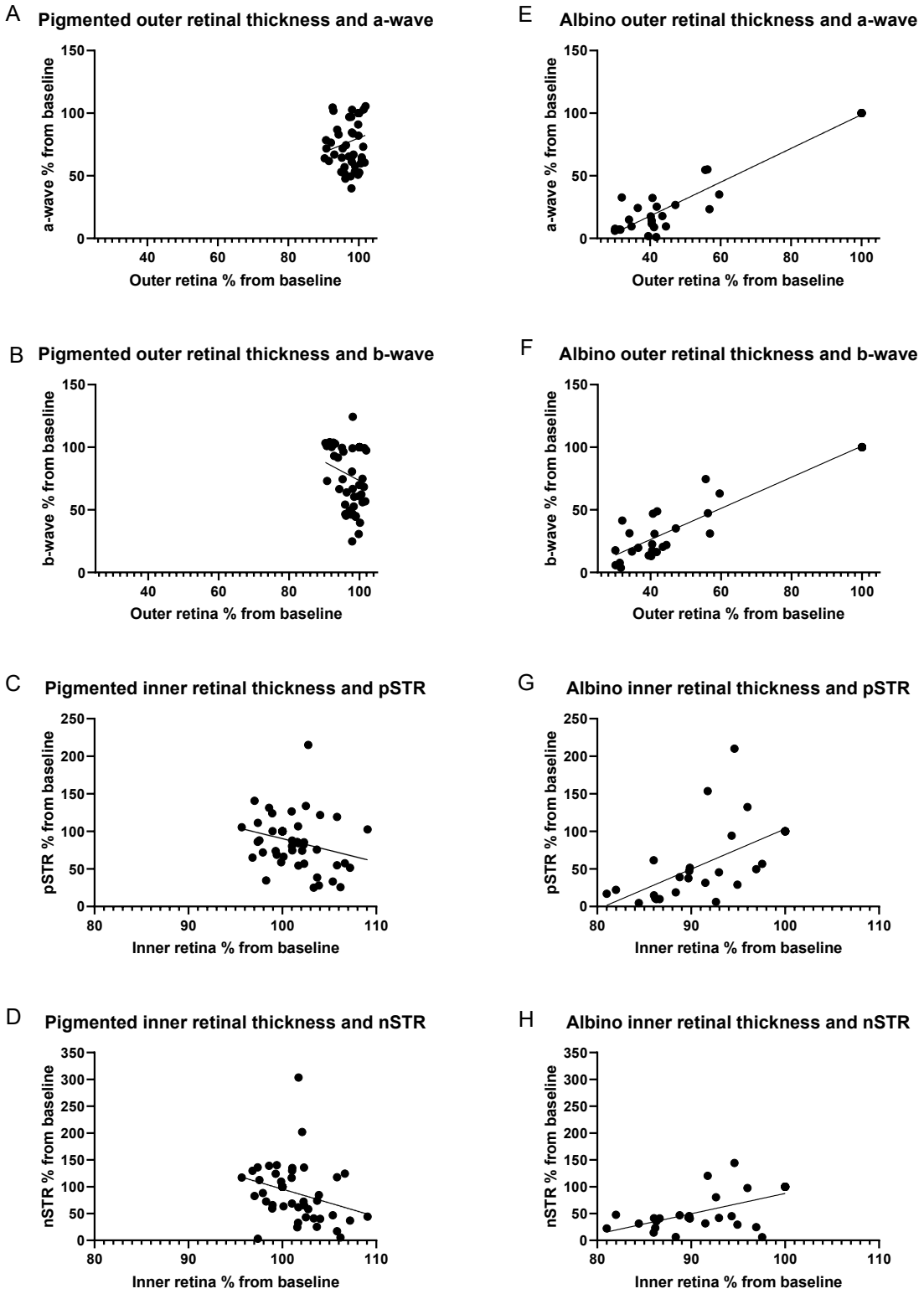

Figure 3-15. Comparisons between retinal thickness and ERG of pigmented (A-D) and albino (E-H) mice. Individual data points are normalized to percent from baseline.

3.7. Immunohistological examination

In pigmented mice, immunohistochemical labelling of outer segment length and cell nuclei in retinal sections appear to be unchanged after LIRD (Figure 3-15). Two-way ANOVA showed no significant effect of time ($p=0.26$) as well as no significant effect of retinal location (superior vs. inferior) ($p=0.27$) on the number of photoreceptor nuclei. Post-hoc analysis (Bonferroni's multiple comparisons test) show no significant difference in photoreceptor nuclei in the superior retina at Day 7 ($p>0.99$), and post-Day 31 ($p=0.22$) compared to control. In the inferior retina, there was no significant difference in Day 7 ($p=0.84$) and post-Day 31 ($p=0.94$) compared to control (Figure 3-16 A).

Two-way ANOVA on outer segment length show a significant effect of time ($p=0.04$) but no significant effect on retinal location ($p=0.36$) in pigmented mice. Although time had a significant effect, post-hoc multiple comparisons test show no significant difference at Day 7 ($p=0.08$) and post-Day 31 ($p=0.98$) compared to control in the superior retina; and no significant difference at Day 7 ($p=0.27$) and post-Day 31 ($p>1.0$) compared to control in the inferior retina (Figure 3-16 B). There was no significant correlation between rows of photoreceptor nuclei and outer segment length in in both the superior (Pearson $r=0.45$, $p=0.06$) and inferior (Pearson $r=0.02$, $p=0.95$) retina (Figure 3-16 C-D).

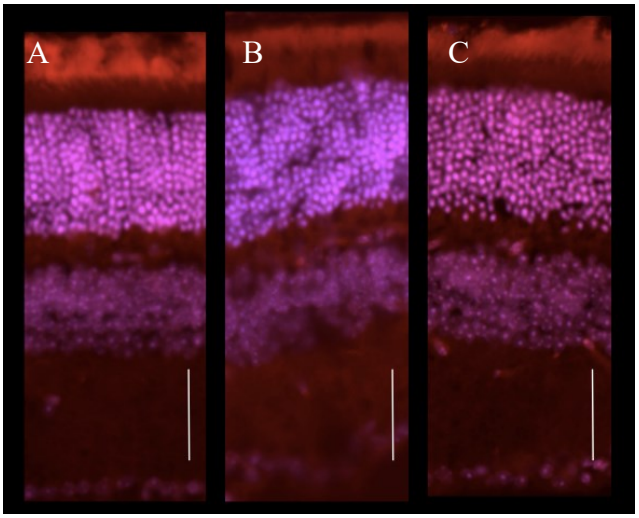

Figure 3-16. Immunohistochemical labelling of outer segments (rhodopsin) and cell nuclei (To-Pro) of pigmented mouse retina sections at (A) 0 days (control), (B) 7 days and (C) 59 days after LIRD. Rhodopsin labelling is observed as red and cell nuclei as pink. Scale bar = 50µm. Magnification = 20x.

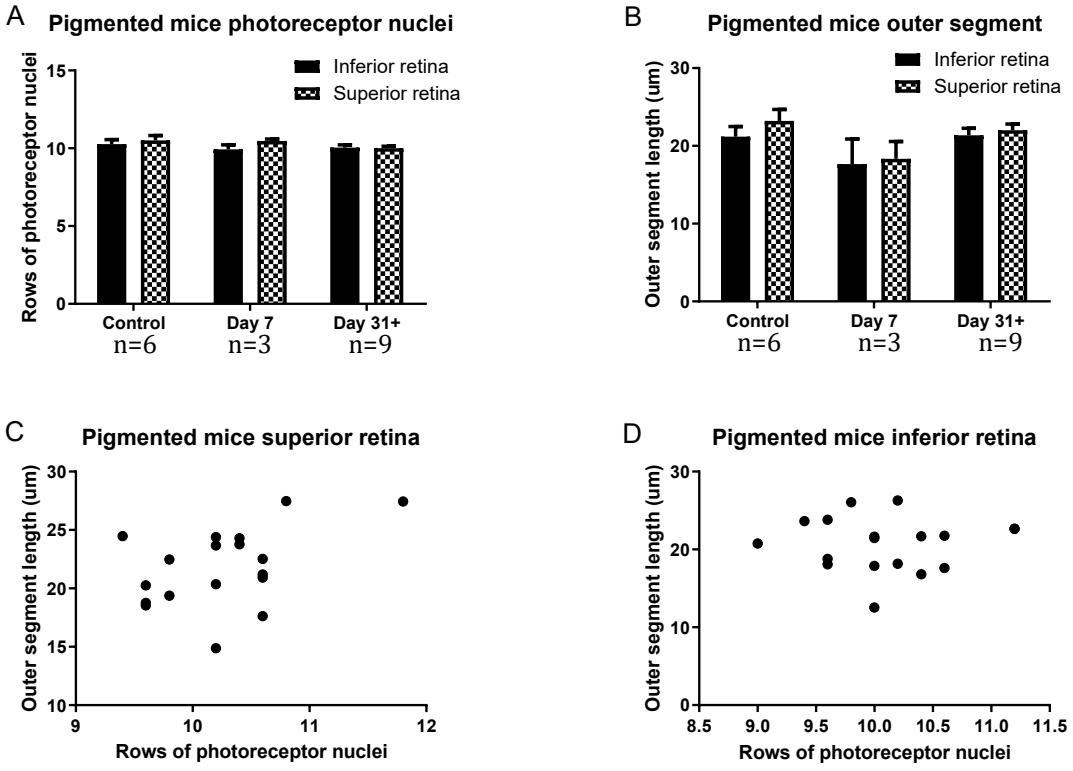

Figure 3-17. (A) Rows of photoreceptor nuclei and (B) outer segment length in pigmented mice. There was no significant relationship between rows of photoreceptor nuclei and outer segment length (C-D).

In albino mice however, immunohistochemical labelling of rhodopsin and cell nuclei appear greatly changed after LIRD (Figure 3-17). 2-way ANOVA showed a significant effect of time ($p<0.01$) on photoreceptor nuclei. There was no significant effect of retinal location ($p=0.53$). Post-hoc multiple comparisons test show a significant difference in photoreceptor nuclei at Day 7 ($p<0.01$) and Day 14+ ($p<0.01$) compared to control in the superior retina. There was also a significant difference in photoreceptor nuclei at Day 7 ($p=0.01$) and Day 14+ ($p<0.01$) compared to control in the inferior retina (Figure 3-18 A).

2-way ANOVA on outer segment length showed a significant effect of time ($p<0.01$) but no significant effect on retinal location ($p=0.62$) in albino mice. Post-hoc multiple comparisons test show a significant difference at Day 7 ($p<0.01$) and post-Day 31 ($p<0.01$) compared to control in both the superior and inferior retina (Figure 3-18 B). There is a significant correlation between rows of photoreceptor nuclei and outer segment length in both the superior (Pearson $r=0.95$, $p<0.01$) and inferior retina (Pearson $r=0.88$, $p<0.01$). The relationships appear to be exponential and were fitted with non-linear curves (Figure 3-18 C-D).

Because there were no differences found between the superior and inferior retinas for photoreceptor nuclei and outer segment length, data were pooled together for comparisons between strains. There was a significant effect of strain found ($p<0.01$) for both photoreceptor nuclei and outer segment lengths.

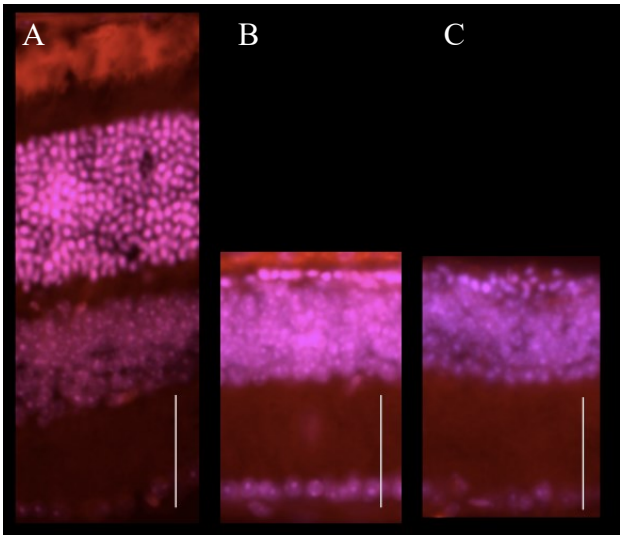

Figure 3-18. Immunohistochemical labelling of outer segment length (rhodopsin) and cell nuclei (To-Pro) of albino mouse retina sections at (A) 0 days (control), (B) 7 days and (C) 62 days after LIRD. Rhodopsin labelling is observed as red and cell nuclei as pink. Scale bar = 50µm. Magnification = 20x.

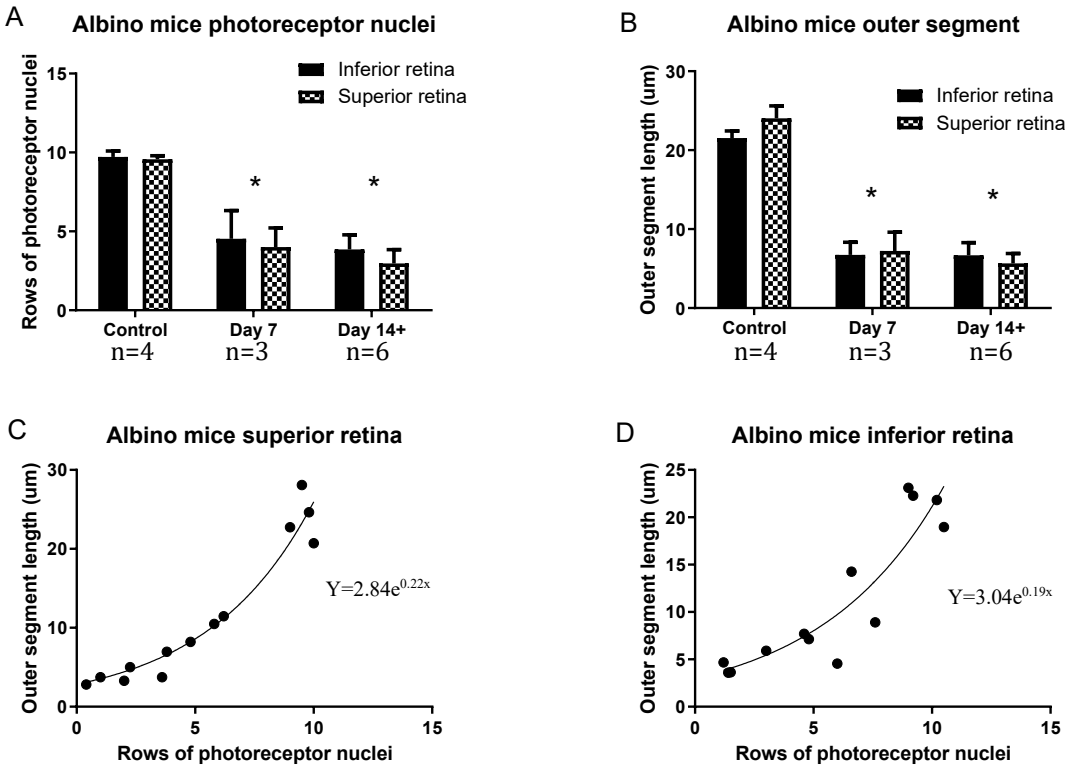

Figure 3-19. (A) Rows of photoreceptor nuclei and (B) outer segment length in albino mice. There appears to be an exponential relationship between rows of photoreceptor nuclei and outer segment length (C-D). Asterisk (*) denote significant difference compared to control.

There was no decrease in RGC density found after LIRD, however 2-way ANOVA of RGC density shows a significant effect of time ($p<0.01$) and mouse strain ($p<0.01$). Post-hoc multiple comparisons test show that RGC density of albino mice at Day 7 ($p=0.01$) and at post-Day 14 ($p<0.01$) was significantly different compared to control. In pigmented mice, there was no significant difference in RGC density at Day 7 ($p=0.73$) and post-Day 14 ($p>0.99$) compared to control (Figure 3-19).

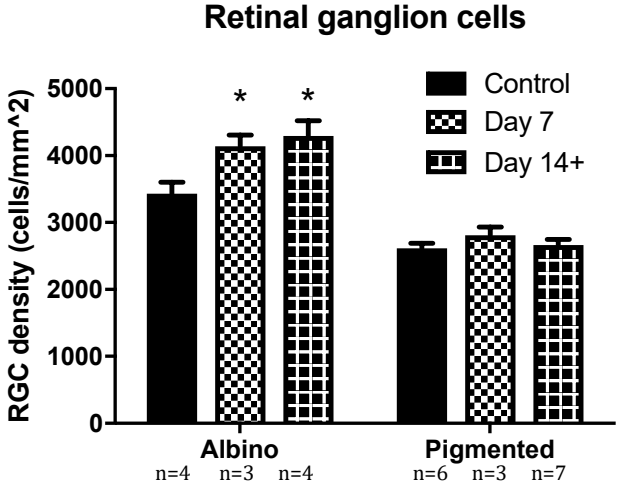

Figure 3-20. Retinal ganglion cell density of albino and pigmented mice. There was no loss of RGC density found in both strains, but the RGC density of LIRD treated albino mice at Day 7 and post-Day 14 were significantly different from the control group. Asterisk (*) denote significant difference compared to control.

4. Chapter 4: Discussion

4.1. Preliminary experiments and designing the experimental protocol

Prior to commencing the LIRD studies, preliminary experiments were performed on pigmented C57BL/6 mice. Two mice for each group were exposed to 18,000 lux for 2, 4, or 6 hours and followed over the course of 16 days. There was no change in retinal thickness in either the outer or inner retina in any animal at Day 16 compared to baseline. Mice that were exposed to 2 and 4 hours of light showed minimal changes in all the ERG waveforms at Day 11 compared to baseline, however those exposed to 6 hours of light showed a small decrease in ERG amplitude in all of the waveforms.

Based on the preliminary data obtained, we decided to use a fluorescent light source with a higher output (22,000 lux) and utilize a longer duration of light exposure (12 hours). With these experimental parameters, we were successful in causing a greater loss in ERG amplitude in all of the waveforms. However, because we were not able to elicit structural loss in retinas of pigmented mice, we decided to include BALB/c albino mice, previously known to show structural changes in the retina after LIRD (Wasowicz et al., 2002; Bhavna et al., 2017).

4.2. The effect of LIRD on retinal structure and function

In our model of LIRD, there was no loss of retinal thickness in either the outer or inner retina in pigmented mice. Subjective OCT studies of pigmented mouse eyes were unchanged before and after LIRD, with all layers appearing distinct and

intact. Immunohistochemical analysis of the retina before and after LIRD showed no change in outer segment length and photoreceptors. The light exposure parameters used for this study have not been sufficient to cause observable damage to the retinal morphology of pigmented mice. In one study, the researchers had to use 70,000 lux exposure over a 50-hour duration to cause ONL loss in pigmented c57/Bl6/J mice (Bai et al., 2012). In contrast, albino mice readily showed a decrease in outer retinal thickness as early as one day after LIRD. Outer retinal thickness continued to decrease by approximately 55% of baseline thickness until Day 7, after which there was minimal change found. Subjective study of the OCT scans of albino mouse eyes showed that inner retinal layers appear largely unchanged after LIRD. The outer retina showed obvious thinning and changes in the reflectivity pattern after LIRD. In particular, the OCT layers between the INL and the RPE become indistinct and are seen as a hyperreflective band that appears to shrink until 7-10 days after LIRD, after which it remains stable. Immunohistochemical analysis showed a large decrease in photoreceptor nuclei and outer segment length after LIRD that was consistent with the thinning of the outer retina found with OCT. No regional differences in outer retinal thickness loss were found in our model of LIRD, unlike in some rat and mouse models where a preferential loss is found in the superior hemisphere of the retina (Montalbán-Soler et al., 2012; Organisciak & Vaughan, 2010). This may be due to differences in methodology. In our LIRD model, we attempted to maximize light exposure by illuminating the animals from all side (from above, the sides and below) whereas other models only utilized illumination from above (e.g. Montalbán-Soler et al., 2012). Indeed it has been found that

changing the light source from above to the sides prevented preferential LIRD loss to the superior retina (Stone et al., 1999). Interestingly, despite no obvious change in the subjective OCT study of inner retinal layers thickness, a gradual thinning of the inner retina, approximately by 10% of baseline thickness, was found over a 62-day period after LIRD. In both pigmented and albino mice, no loss of RGC densities were found after LIRD. Interestingly, we found an increase in RGC density in albino mice post-LIRD. However, given the unlikely scenario of spontaneous growth of new RGCs after LIRD, this is likely due to individual variations and a small n and not due to an actual increase in RGC density.

Unsurprisingly, there was a much larger decrease in retinal function of albino mice compared to pigmented mice, and this was true for all ERG waveforms analyzed. The large decrease in photoreceptor cells (approximately 60% loss by the end of the experiment) certainly corresponds to the larger decrease in a- and b-wave responses, and subsequently affects the downstream STR responses. In addition, the apparent thinning of the inner retina observed in albino mouse may also contribute to the larger STR reduction compared to what was observed in pigmented mice, although which cells are affected and the underlying mechanisms are still unknown.

In both of our pigmented and albino mouse LIRD models, an overall decrease in retinal function was found with no recovery in all waveforms. This is unlike the findings of Montalbán-Soler and colleagues (2012), where LIRD in albino BALB/c mice caused an initial decrease in the a-wave, b-wave, pSTR and nSTR, followed by partial recovery of the a- and b-waves, and complete recovery of the STRs. It is

worth noting that the parameters of light exposure between our study and theirs are different. In their cross-sectional study, mice were exposed to 3,000 lux (compared to 22,000 lux in our experiment) over a course of 24 hours (compared to 12 hours in our experiment). It is probable that the higher light intensity used in our study crossed a damage threshold where functional recovery cannot occur. It is interesting however that the results of our study show an initial decrease in ERG amplitudes followed by what appears to be possible transient recovery after Day 14 post-LIRD, especially for pigmented mice. The ERG results post-Day 14 show significant fluctuation, but the overall trend points to reduced retinal function with no recovery. Because our mice were followed longitudinally, they were subjected to repeated ketamine-xylazine injections. It is plausible that repeated exposure to anesthesia can cause desensitization, leading to animals being more shallowly anesthetized and resulting in fluctuations in ERG recordings. Indeed, it was observed during the experiments that mice that underwent multiple sessions with anesthesia took longer for sufficiently deep anesthesia and remained in that state for shorter periods.

4.3. Correlation between ERG waveforms and retinal thickness

The relationship between ERG waveforms and retinal thickness were examined. The individual panels in Figure 3-13 were overlaid with a line of slope = 1 indicating a perfect linear relationship. In both albino and pigmented mice, there was an almost 1:1 proportion change in the a- and b-wave; in other words, any loss in a-wave amplitude would result in a proportional loss in the b-wave amplitude. In the comparisons between the a-wave and the STRs, many of the individual data points fall above the line of slope = 1, This indicates that there was less reduction in both pSTR and nSTR compared to reductions in the a-wave, suggesting an underlying compensatory mechanism at the level of the inner retina. Comparisons of the slopes, intercepts and residual plots of the relationship between the a-wave vs. b-wave to the a-wave vs. the STRs also showed a similar difference.

Comparing retinal thickness loss to ERG amplitude in albino mice, it is unsurprising that decreased outer and inner retinal thickness correspond to decreased ERG amplitudes. Since there was no loss of retinal thickness in pigmented mice, it was difficult to make any comparisons between retinal thickness and ERG amplitude. It is interesting however that in spite of the outer and inner retina of pigmented mice remaining intact, there appeared to be a permanent reduction in retinal function. A reduction in the amount of rhodopsin could explain the reduction in ERG amplitudes, although experiments on recovery from LIRD show that ERG sensitivity is restored when outer segment discs (containing rhodopsin) are regenerated (Rapp & Williams, 1977). Although we did not specifically measure rhodopsin expression (i.e. through Western Blot or other methods), there was no

change in outer segment length (and no change on the labelled rhodopsin) found in pigmented mice after LIRD compared to control mice. This suggests that depletion of rhodopsin is unlikely the cause of the permanent ERG reductions in pigmented mice. Another possibility causing reduction of ERGs despite no structural loss is retinal remodeling that occurs after LIRD. Changes in synaptic connections and neuronal cell migration have been found in rat LIRD (Marc et al., 2008) and photoreceptor degeneration models (Jones et al., 2003) and may potentially account for ERG reductions.

4.4. Strain differences in LIRD

Our model of LIRD showed a much larger effect of light damage on the retinal structures and function of albino mice compared to pigmented mice, suggesting that pigmentation protects the retina from LIRD. Ocular pigments such as melanin in the RPE protects against LIRD by reducing damage to retinal cells caused by oxidative stress (Priglinger et al., 2003). However, pigmentation does not confer more protection against LIRD in all cases. Research involving Long-Evans (pigmented) and Wistar (albino) rats showed a structural loss of photoreceptor cells as well as evidence of apoptosis in both nuclear layers and the ganglion cell layer after LIRD (Wasowicz et al., 2002). In contrast, a study comparing Wistar (albino) and Brown-Norway (pigmented) rats showed similar outer retinal structural losses in both strains, but more functional ERG damage in Brown-Norway rats (Tremblay et al., 2013). A comparison of LIRD between Long-Evans (pigmented), Brown-Norway (pigmented), Sprague Dawley (albino) and Lewis (albino) rats showed that Brown-

Norway rats showed the most damage from LIRD, followed by Sprague Dawley and Lewis rats. Long-Evans rats showed the least damage of the four strains (Polosa et al., 2016). In mice, two phenotypically identical albino strains with different genetic background (BALB/cByJ and C57BL/6J-c2J mice) can show vastly different effects of LIRD to the outer retina (LaVail et al., 1987). The above works cited suggests that genetic background, in addition to ocular pigmentation, is an important indicator of susceptibility to LIRD.

4.5. Limitations and future directions

Because of the difficulty in manually segmenting the individual layers of the outer retina post-LIRD, we decided to limit the OCT analyses of the retinal structure to the outer retina and inner retina as a whole. The individual layers of the inner retina though appear intact after LIRD, and it would be interesting to find out which layer within the albino inner retina is reduced and when the thinning occurs after LIRD,. The next step would be to manually segment and analyze each layer of the inner retina to find out if the thinning occurs within the RNFL, GCL or IPL.

One limitation of this study is that the repeated anesthetic injections likely caused desensitization, resulting in the animal reaching a shallower plane of anesthesia and subsequent fluctuations in ERG recording. Increasing the anesthetic dosage may be helpful in combatting desensitization to the anesthesia, however, at the increased risk of overdose. A study on the proper titration of anesthetic dose would be beneficial in future longitudinal ERG studies.

The OCT is an excellent tool for monitoring *in vivo* morphological changes in the retina. Eye tracking software in particular is especially helpful in pinpointing areas where subtle retinal changes can occur. This study is limited in that it was not possible to utilize eye tracking at all times. Unclear ocular media and excessive ocular torsion sometimes resulted in difficulties registering the eye tracking software.

4.6. Conclusion

In mice, permanent functional loss in the retina can occur even in the absence of morphological damage during LIRD. The a-wave, b-wave and STRs were decreased after LIRD, despite no measurable changes in retinal thickness in pigmented mice. Retinal thickness loss due to LIRD in albino mice results in increased functional deficits in both the inner and outer retina. Functional deficits of the inner retina however, are decreased compared to functional deficits of the outer retina, suggesting an underlying functional compensatory mechanisms at the level of the inner retina.

References

Alarcón-Martínez, L., Villa, d. L., Aviles-Trigueros, M., Blanco, R., Villegas-Perez, M., & Vidal-Sanz, M. (2009). Short and long term axotomy-induced ERG changes in albino and pigmented rats. *Molecular Vision, 15*(254-55), 2373-2383.

Alarcón-Martínez, L., Avilés-Trigueros, M., Galindo-Romero, C., Valiente-Soriano, J., Agudo-Barriuso, M., Villa, P., Villegas-Pérez, M. & Vidal-Sanz, M. (2010). ERG changes in albino and pigmented mice after optic nerve transection. *Vision Research, 50*(21), 2176-2187.

Bai, S., Sheline, C. R., Zhou, Y., & Sheline, C. T. (2012). A reduced zinc diet or zinc transporter 3 knockout attenuate light induced zinc accumulation and retinal degeneration. *Experimental Eye Research, 108*, 59-67.

Baker, S. A., & Kerov, V. (2013). Chapter seven - photoreceptor inner and outer segments. In V. Bennett (Ed.), *Current topics in membranes* (pp. 231-265) Academic Press. doi:https://doi.org/10.1016/B978-0-12-417027-8.00007-6 Retrieved from http://www.sciencedirect.com/science/article/pii/B9780124170278000076.

Bhavna, J. A., Kim, B. J., Lang, A., Carass, A., Jerry, L. P., & Donald, J. Z. (2017). Automated segmentation of mouse OCT volumes (ASiMOV): Validation & clinical study of a light damage model. *Plos One, 12*(8), e0181059. doi:10.1371/journal.pone.0181059.

Brown, K. T., & Wiesel, T. N. (1961). Localization of origins of electroretinogram components by intraretinal recording in the intact cat eye. *The Journal of Physiology, 158*(2), 257-280. doi:10.1113/jphysiol.1961.sp006768.

Chauhan, B. C., Stevens, K. T., Levesque, J. M., Nuschke, A. C., Sharpe, G. P., O'Leary, N., Archibald, M. & Wang, X. (2012). Longitudinal in vivo imaging of retinal ganglion cells and retinal thickness changes following optic nerve injury in mice. *Plos One, 7*(6), e40352. Retrieved from https://doi.org/10.1371/journal.pone.0040352.

Do, M., Kang, S., Xue, T., Zhong, H., Liao, H., Bergles, D. & Yau, K. (2008). Photon capture and signalling by melanopsin retinal ganglion cells. *Nature, 457*(7227), 281-7.

Faul, F., Erdfelder, E., Lang, A. G., & Buchner, A. (2007). G*Power 3: A flexible statistical power analysis program for the social, behavioral, and biomedical sciences. *Behavior Research Methods, 39*(2), 175-191.

Faul, F., Erdfelder, E., Buchner, A., & Lang, A. (2009). Statistical power analyses using G*Power 3.1: Tests for correlation and regression analyses. *Behavior Research Methods, 41*(4), 1149-1160. doi:10.3758/BRM.41.4.1149.

Ferguson, L., Dominguez II, J., Balaiya, S., Grover, S., Chalam, K., & Villoslada, P. (2013). Retinal Thickness Normative Data in Wild-Type Mice Using Customized Miniature SD-OCT. *PLoS ONE, 8*(6), E67265.

Forrester, J. V., Dick, A. D., McMenamin, P. G., Roberts, F., & Pearlman, E. (2016). Chapter 5 - physiology of vision and the visual system. In J. V. Forrester, A. D. Dick, P. G. McMenamin, F. Roberts & E. Pearlman (Eds.), *The eye (fourth edition)* (pp. 269-337.e2) W.B. Saunders. doi:https://doi.org/10.1016/B978-0-7020-5554-6.00005-8 Retrieved from http://www.sciencedirect.com/science/article/pii/B9780702055546000058.

Frishman, L. J. (2013). Chapter 7 - electrogenesis of the electroretinogram. In S. J. Ryan, S. R. Sadda, D. R. Hinton, A. P. Schachat, C. P. Wilkinson & P. Wiedemann (Eds.), *Retina* (5th ed., pp. 177-201). London: W.B. Saunders. doi:https://doi.org/10.1016/B978-1-4557-0737-9.00007-2 Retrieved from http://www.sciencedirect.com/science/article/pii/B9781455707379000072.

Frishman, L. J., & Wang, M. H. (2011). Electroretinogram of human, monkey and mouse. In L. A. Levin, & F. H. Adler (Eds.), *Adler's physiology of the eye* (11th ed. ed., pp. 480-501). Edingburg: Saunders/Elsevier.

Ganekal, S., Dorairaj, S., & Jhanji, V. (2013). Pattern Electroretinography Changes in Patients with Established or Suspected Primary Open Angle Glaucoma. *Journal of Current Glaucoma Practice, 7*(2), 39-42.

García-Ayuso, D., Salinas-Navarro, M., Agudo-Barriuso, M., Alarcón-Martínez, L., Vidal-Sanz, M., & Villegas-Pérez, M. P. (2011). Retinal ganglion cell axonal compression by retinal vessels in light-induced retinal degeneration. *Molecular Vision, 17*, 1716-1733.

Gregg, R. G., McCall, M. A., & Massey, S. C. (2013). Chapter 15 - function and anatomy of the mammalian retina. In S. J. Ryan, S. R. Sadda, D. R. Hinton, A. P. Schachat, C. P. Wilkinson & P. Wiedemann (Eds.), *Retina* (5th ed., pp. 360-400). London: W.B. Saunders. doi:https://doi.org/10.1016/B978-1-4557-0737-9.00015-1 Retrieved from http://www.sciencedirect.com/science/article/pii/B9781455707379000151.

Grimm, C., Wenzel, A., Hafezi, F., Yu, S., Michael Redmond, T., & Rem, C. E. (2000). Protection of Rpe65-deficient mice identifies rhodopsin as a mediator of light-induced retinal degeneration. *Nature Genetics, 25*(1), 63. doi:10.1038/75614.

Grimm, C., Wenzel, A., Williams, T., Rol, P., Hafezi, F., & Remé, C. (2001). Rhodopsin-mediated blue-light damage to the rat retina: Effect of photoreversal of bleaching. *Investigative Ophthalmology & Visual Science, 42*(2), 497.

Grimm, C., & Remé, C.E. (2013). Light damage as a model of retinal degeneration. *Methods in Molecular Biology (Clifton, N.J.), 935*, 87. doi:10.1007/978-1-62703-080-9_6.

Gotoh, Y., Machida, S., & Tazawa, Y. (2004). Selective Loss of the Photopic Negative Response in Patients With Optic Nerve Atrophy. *Archives of Ophthalmology, 122*(3), 341-6.

Hattar, S., Liao, H., Takao, M., Berson, D., & Yau, K. (2002). Melanopsin-containing retinal ganglion cells: Architecture, projections, and intrinsic photosensitivity. *Science (New York, N.Y.), 295*(5557), 1065-1070.

Huang, D., Swanson, E., Lin, C., Schuman, J., Stinson, W., Chang, W., Hee, M., Flotte, T., Gregory, K., Puliafito, C., & Fujimoto, J. (1991). Optical coherence tomography. *Science (New York, N.Y.), 254*(5035), 1178-1181.

Jiménez-Sierra, J. M., Ogden, T. E., & Van Boemel, G. B. (1989). *Inherited retinal diseases : A diagnostic guide*. St. Louis, MO: Mosby.

Jones, B., Watt, C., Frederick, J., Baehr, W., Chen, C., Levine, E., . . . Marc, R. (2003). Retinal remodeling triggered by photoreceptor degenerations. *Journal of Comparative Neurology, 464*(1), 1-16.

Kolb, H. (2003). How the retina works. *American Scientist, 91*(1), 28-35. doi:10.1511/2003.1.28..

Kolb, H. (2007). Facts and figures concerning the human retina. Retrieved from https://www.ncbi.nlm.nih.gov/books/NBK11556/.

Korth, M., Nguyen, N., Horn, F., & Martus, P. (1994). Scotopic threshold response and scotopic PII in glaucoma. *Investigative Ophthalmology & Visual Science,35*(2), 619-625.

Kuwabara, T., & Gorn, R. A. (1968). Retinal damage by visible light. an electron microscopic study. *Archives of Ophthalmology (Chicago, Ill.: 1960), 79*(1), 69. doi:10.1001/archopht.1968.03850040071019.

LaVail, M., Gorrin, G., Repaci, M., Thomas, L., & Ginsberg, H. (1987). Genetic regulation of light damage to photoreceptors. *Investigative Ophthalmology & Visual Science, 28*(7), 1043-1048.

Levin, L. A., & Gordon, L. K. (2002). Retinal ganglion cell disorders: Types and treatments. *Progress in Retinal and Eye Research, 21*(5), 465-484. doi:10.1016/S1350-9462(02)00012-5.

Marc, R., Jones, B., Watt, C., Vazquez-Chona, F., Vaughan, D., & Organisciak, D. (2008). Extreme retinal remodeling triggered by light damage: Implications for age related macular degeneration. *Molecular Vision, 14*, 782-806.

Marco-Gomariz, M., Hurtado-Montalbán, N., Vidal-Sanz, M., Lund, R., & Villegas-Pérez, M. (2006). Phototoxic-induced photoreceptor degeneration causes retinal ganglion cell degeneration in pigmented rats. *Journal of Comparative Neurology, 498*(2), 163-179.

Miceli, M., Liles, M., & Newsome, D. (1994). Evaluation of Oxidative Processes in Human Pigment Epithelial Cells Associated with Retinal Outer Segment Phagocytosis. *Experimental Cell Research, 214*(1), 242-249.

Molday, R. S. (1998). Photoreceptor membrane proteins, phototransduction, and retinal degenerative diseases. the friedenwald lecture. *Investigative Ophthalmology & Visual Science, 39*(13), 2491-2513.

Montalbán-Soler, L., Alarcón-Martínez, L., Jiménez-López, M., Salinas-Navarro, M., Galindo-Romero, C., Bezerra, d. S., Garcia-Ayuso, D. Avilés-Trigueros, M., Vidal-Sanz, M., Agudo-Barriuso, M., & Villegas-Pérez, M.,P. (2012). Retinal compensatory changes after light damage in albino mice. *Molecular Vision, 18*, 675.

Noell, W. K., Walker, V. S., Kang, B. S., & Berman, S. (1966). Retinal damage by light in rats. *Investigative Ophthalmology, 5*(5), 450.

Organisciak, & Vaughan. (2010). Retinal light damage: Mechanisms and protection. *Progress in Retinal and Eye Research, 29*(2), 113-134.

O' Steen, W. K., Shear, C. R., & Anderson, K. V. (1972). Retinal damage after prolonged exposure to visible light. A light and electron microscopic study. *American Journal of Anatomy, 134*(1), 5-21. doi:10.1002/aja.1001340103.

Palczewski, K. (2014). Chemistry and biology of the initial steps in vision: The friedenwald lecture. *Investigative Ophthalmology & Visual Science, 55*(10), 6651-6672. doi:10.1167/iovs.14-15502.

Park, P. S. (2014). Constitutively active rhodopsin and retinal disease. *Advances in Pharmacology (San Diego, Calif.), 70*, 1-36. doi:10.1016/B978-0-12-417197-8.00001-8.

Pinto, L., Invergo, B., Shimomura, K., Takahashi, J., & Troy, J. (2007). Interpretation of the mouse electroretinogram. *Documenta Ophthalmologica; the Journal of Clinical Electrophysiology and Vision - the Official Journal of the International Society for Clinical Electrophysiology and Vision, 115*(3), 127-136. doi:10.1007/s10633-007-9064-y.

Pepperberg, D. R., Brown, P. K., Lurie, M., & Dowling, J. E. (1978). Visual pigment and photoreceptor sensitivity in the isolated skate retina. *The Journal of General Physiology, 71*(4), 369-396. Retrieved from http://www.ncbi.nlm.nih.gov/pmc/articles/PMC2215732/.

Perlman, I. (2018). The electroretinogram: ERG by ido perlman. Retrieved from https://webvision.med.utah.edu/book/electrophysiology/the-electroretinogram-erg/..

Polosa, A., Bessaklia, H., & Lachapelle, P. (2017). Light-induced retinopathy: Young age protects more than ocular pigmentation. *Current Eye Research, 42*(6), 924-935. doi:10.1080/02713683.2016.1255336.

Priglinger, S., Alge, C., Neubauer, A., Kunze, C., Kampik, A., & Welge-Lussen, U. (2003). Melanin protects cultured retinal pigment epithelial (RPE) cells from oxidative stress. *Investigative Ophthalmology & Visual Science, 44*, U384.

Purves, D., & Williams, S. M. (2004). *Neuroscience* (3rd ed.. ed.). Sunderland, Mass.: Sunderland, Mass. : Sinauer Associates.

Putting, B. J., Van Best, J. A., Vrensen, G. F. J. M., & Oosterhuis, J. A. (1994). Blue-light-induced dysfunction of the blood-retinal barrier at the pigment epithelium in albino versus pigmented rabbits. *Experimental Eye Research, 58*(1), 31-40. doi:10.1006/exer.1994.1192.

Rapp, L. & Williams, T. (1977). Rhodopsin content and electroretinographic sensitivity in light-damaged rat retina. *Nature, 267*(5614), 835-6.

Rastogi, V., Puri, N., Arora, S., Kaur, G., Yadav, L., & Sharma, R. (2013). Artefacts: A diagnostic dilemma - A review. *Journal of Clinical and Diagnostic Research, 7*(10), 2408-2413. doi:10.7860/JCDR/2013/6170.3541.

Remé, C., Reinboth, J., Clausen, M., & Hafezi, F. (1996). Light damage revisited: Converging evidence, diverging views? *Graefe's Archive for Clinical and Experimental Ophthalmology, 234*(1), 2-11.

Remé, Grimm, Hafezi, Marti, & Wenzel. (1998). Apoptotic cell death in retinal degenerations. *Progress in Retinal and Eye Research, 17*(4), 443-464.

Remington, L. A. (2012). Chapter 4 - Retina. In L. A. Remington (Ed.), *Clinical anatomy and physiology of the visual system* (3rd ed., pp. 61-92). Saint Louis: Butterworth-Heinemann. doi:https://doi-org.ezproxy.library.dal.ca/10.1016/B978-1-4377-1926-0.10004-9.

Reuter, J. H., & Hobbelen, J. F. (1977). *The effect of continuous light exposure on the retina in albino and pigmented rats* doi:https://doi.org/10.1016/0031-9384(77)90204-9.

Rodriguez, A. R., Sevilla Müller, L. P., & Brecha, N. C. (2014). The RNA binding protein RBPMS is a selective marker of ganglion cells in the mammalian retina. *Journal of Comparative Neurology, 522*(6), 1411-1443. doi:10.1002/cne.23521.

Saenz-de-Viteri, M., Heras-Mulero, H., Fernández-Robredo, P., Recalde, S., Hernández, M., Reiter, N., & García-Layana, A. (2014). Oxidative Stress and Histological Changes in a Model of Retinal Phototoxicity in Rabbits. *Oxidative Medicine and Cellular Longevity, 2014*, 10.

Saszik, S. M., Robson, J. G., & Frishman, L. J. (2002). The scotopic threshold response of the Dark-Adapted electroretinogram of the mouse. *Journal of Physiology, 543*(3), 899-916. doi:10.1113/jphysiol.2002.019703.

Sharma, R. K., & Ehinger, B. E. J. (2003). Development and structure of the retina. In P. L. Kaufman, & A. Alm (Eds.), *Adler's physiology of the eye* (10th ed., pp. 319). St Louis: Mosby.

Smith, B. J., Wang, X., Chauhan, B. C., Côté, P. D., & Tremblay, F. (2014). Contribution of retinal ganglion cells to the mouse electroretinogram. *Documenta Ophthalmologica, 128*(3), 155-168. doi:10.1007/s10633-014-9433-2.

Sieving, P. A., Frishman, L. J., & Steinberg, R. H. (1986). Scotopic threshold response of proximal retina in cat. *Journal of Neurophysiology, 56*(4), 1049. doi:10.1152/jn.1986.56.4.1049.

Sieving, P. A. (1991). Scotopic threshold response of the electroretinogram. In J. R. Heckenlively, & G. B. Arden (Eds.), *Principles and practice of clinical electrophysiology of vision* (pp. 352-362). St. Louis, MO: Mosby-Year Book.

Stone, J., Maslim, J., Valter-Kocsi, K., Kyle Mervin, F., Bowers, Y, Chu, N., Barnett, J., Provis, G., Lewis, S.,Fisher, S., Bisti, C., Gargini, L., Cervetto, S.,Merin, J. & Pe'Er, J. (1999). Mechanisms of photoreceptor death and survival in mammalian retina. Progress in Retinal and Eye Research, 18(6), 689-735.

Sugawara, T., Sieving, P. A., & Bush, R. A. (2000). Quantitative relationship of the scotopic and photopic ERG to photoreceptor cell loss in light damaged rats. *Experimental Eye Research, 70*(5), 693-705. doi:10.1006/exer.2000.0842.

Tanito, M., Kaidzu, S., Ohira, A. & Anderson, R. (2008). Topography of retinal damage in light-exposed albino rats. *Experimental Eye Research, 87*(3), 292-295.

Thumann, G., Dou, G., Wang, Y., & Hinton, D. R. (2013). Chapter 16 - cell biology of the retinal pigment epithelium. In S. J. Ryan, S. R. Sadda, D. R. Hinton, A. P. Schachat, C. P. Wilkinson & P. Wiedemann (Eds.), *Retina* (5th ed., pp. 401-414). London: W.B. Saunders. doi:https://doi.org/10.1016/B978-1-4557-0737-9.00016-3 Retrieved from http://www.sciencedirect.com/science/article/pii/B9781455707379000163.

Toda, K., Bush, R. A., Humphries, P., & Sieving, P. A. (1999). The electroretinogram of the rhodopsin knockout mouse. *Visual Neuroscience, 16*(2), 391-398. doi:10.1017/S0952523899162187.

Tremblay, F., Waterhouse, J., Nason, J., & Kalt, W. (2013). Prophylactic neuroprotection by blueberry-enriched diet in a rat model of light-induced retinopathy. *Journal of Nutritional Biochemistry, 24*(4), 647-655.

Vicente-Tejedor, J., Marchena, M., Ramírez, L., García-Ayuso, D., Gómez-Vicente, V., Sánchez-Ramos, C., de La Villa, P., Germain, F. (2018). Removal of the blue component of light significantly decreases retinal damage after high intensity exposure. *PloS One, 13*(3), E0194218.

Volland, S., Esteve-Rudd, J., Hoo, J., Yee, C., & Williams, D. S. (2015). A comparison of some organizational characteristics of the mouse central retina and the human macula. *Plos One, 10*(4), e0125631. Retrieved from https://doi.org/10.1371/journal.pone.0125631.

Wang, K., Xiao, J., Peng, B., Xing, F., So, K., Tipoe, G., & Lin, B. (2014). Retinal structure and function preservation by polysaccharides of wolfberry in a mouse model of retinal degeneration. *Scientific Reports, 4*, 7601.

Wasowicz, M., Morice, C., Ferrari, P., Callebert, J., & Versaux-Botteri, C. (2002). Long-term effects of light damage on the retina of albino and pigmented rats. *Investigative Ophthalmology & Visual Science, 43*(3), 813-820.

Wenzel, A., Reme, C., Williams, T., Hafezi, F., & Grimm, C. (2001). The Rpe65 Leu450Met Variation Increases Retinal Resistance Against Light-Induced Degeneration by Slowing Rhodopsin Regeneration. *Journal of Neuroscience, 21*(1), 53-58.

Westheimer, G. (2007). The ON–OFF dichotomy in visual processing: From receptors to perception. *Progress in Retinal and Eye Research, 26*(6), 636-648. doi:10.1016/j.preteyeres.2007.07.003.

Youssef, P. N., Sheibani, N., & Albert, D. M. (2010). Retinal light toxicity. *Eye, 25*(1), 1. doi:10.1038/eye.2010.149.

Appendix A. Total n (number of eyes) collected for each timepoint (day) for pigmented mice.

Day	ERG (n)	OCT (n)
Baseline	19	10
1		2
3		12
7	19	2
10		10
14	18	
17		10
21	9	
22	4	
23	2	
25		9
28	2	
29	8	
31		7
35	2	
37	4	
43		2
59		5
62		1
68	4	
73	2	
81	10	
117		1
121	10	

Appendix B. Total n (number of eyes) collected for each timepoint (day) for albino mice.

Day	ERG (n)	OCT (n)
Baseline	12	6
1		5
3		10
7	12	5
10		5
14	12	
17		6
21	10	
24		5
31		2
35	2	
37	6	
42		3
62		3
68	6	
73	2	

Appendix C. Permission to Reprint

Dear Justine Sy

We hereby grant you permission to reprint the material below at no charge **in your thesis** subject to the following conditions:

1. If any part of the material to be used (for example, figures) has appeared in our publication with credit or acknowledgement to another source, permission must also be sought from that source. If such permission is not obtained then that material may not be included in your publication/copies.
2. Suitable acknowledgment to the source must be made, either as a footnote or in a reference list at the end of your publication, as follows:

   "This article was published in Publication title, Vol number, Author(s), Title of article, Page Nos, Copyright Elsevier (or appropriate Society name) (Year)."

3. Your thesis may be submitted to your institution in either print or electronic form.
4. Reproduction of this material is confined to the purpose for which permission is hereby given.
5. This permission is granted for non-exclusive world **English** rights only. For other languages please reapply separately for each one required.
6. Permission excludes use in an electronic form other than submission. Should you have a specific electronic project in mind please reapply for permission.
7. Should your thesis be published commercially, please reapply for permission. This includes permission for the Library and Archives of Canada to supply single copies, on demand, of the complete thesis. Should your thesis be published commercially, please reapply for permission.

Thanks
Akshaya

Akshaya G R
Copyrights Coordinator, GR - Copyrights
ELSEVIER | Global Book Production
+91 44 4299 4930 office
a.ganesh.1@elsevier.com

From: Justine.Sy@dal.ca [mailto:Justine.Sy@dal.ca]
Sent: Friday, September 7, 2018 6:18 AM
To: Rights and Permissions (ELS) <Permissions@elsevier.com>
Subject: Obtain permission request - Book

***** External email: use caution *****

Title: Ms. Justine Sy

Institute/company: Dalhousie University
Address: 219 Green Village Lane
Post/Zip Code: B2Y 4V5
City: Dartmouth
State/Territory: Nova Scotia
Country: Canada
Telephone: 9024039680
Email: Justine.Sy@dal.ca

Type of Publication: Book

Book Title:Clinical Anatomy and Physiology of the Visual System
Book ISBN: 9781437719260
Book Author: Lee Ann Remington
Book Year: 2012
Book Pages: 71 to 72
Book Chapter number: 4
Book Chapter title: Retina

I would like to use: Figure(s)
Quantity of material: 2
Excerpts:

Are you the author of the Elsevier material? No

If not, is the Elsevier author involved? No

If yes, please provide details of how the Elsevier author is involved:

In what format will you use the material? Print and Electronic

Will you be translating the material? No

If yes, specify language:

Information about proposed use: Reuse in a thesis/dissertation
Proposed use text: N/A

Additional Comments / Information: Requesting permission to use Figures 4-11 and 4-13